Final Report

Project Title: Mechanistic Model for Analysis of Nano-scale Beams and Rectangular Plates with Surface Stress Effects

By Yasothorn Sapsathiarn Mahidol University

July/ 2016

Contract No. TRG5780139

Final Report

Project Title: Mechanistic Model for Analysis of Nano-scale Beams and Rectangular Plates with Surface Stress Effects

Researcher	Institute
Yasothorn Sapsathiarn	Mahidol University

This project granted by the Thailand Research Fund

Abstract

Project Code : TRG5780139

Project Title : Mechanistic Model for Analysis of Nano-scale Beams and Rectangular Plates with Surface Stress Effects

Investigator : Yasothorn Sapsathiarn
Department of Civil and Environmental Engineering
Faculty of Engineering, Mahidol University
25/25 Puttamonthon 4 Road
Salaya, Nakornpathom 73170

E-mail Address : yasothorn.sap@mahidol.ac.th

Project Period : 2 years

Abstract: Nanotechnology is a frontier revolutionary technology that offers a wide range of promising applications such as computers, electronics, medical devices, etc. The development of nanotechnology applications requires an understanding of responses of nano-scale structures such as nanobeams/wires, nanotubes, nanoparticles and nanoplates, which are the key components of nano-scale devices. The proposed research investigation is motivated by the need to develop a suitable theoretical model to analyze the complex behavior of nano-scale beams and plates observed in experiments. Mechanistic models incorporating surface stress effects are proposed to be developed during this investigation and applied to examine the influence of size effects and boundary conditions on nanobeam and nanoplate responses. The outcomes from the proposed investigation are expected to provide a novel insight into the complex size-dependent behavior of nanobeams and nanoplates. This knowledge is crucial for the nanotechnology researchers and engineers to produce reliable designs of nano-scale devices and nanotechnology applications.

Keywords : Nanotechnology; Mechanistic model; Nanobeams/plates; Surface energy

Final report

TRF Grant for New Researcher

Project title:(English) Mechanistic Model for Analysis of Nano-scale Beams and Rectangular Plates with Surface Stress Effects

(Thai) แบบจำลองทางกลศาสตร์สำหรับการวิเคราะห์คานและแผ่นพื้นสี่เหลี่ยมขนาดนาโนโดยคำนึงถึงอิทธิพลของหน่วยแรงที่ผิว

1. Abstract

(English) Nanotechnology is a frontier revolutionary technology that offers a wide range of promising applications such as computers, electronics, medical devices, etc. The development of nanotechnology applications requires an understanding of responses of nano-scale structures such as nanobeams/wires, nanotubes, nanoparticles and nanoplates, which are the key components of nano-scale devices. The present research investigation is motivated by the need to develop a suitable theoretical model to analyze the complex behavior of nano-scale beams and plates observed in experiments. Mechanistic models incorporating surface stress effects are developed during this investigation and applied to examine the influence of size effects and boundary conditions on nanobeam and nanoplate responses. The outcomes from the present research investigation provide a novel insight into the complex size-dependent behavior of nanobeams and nanoplates. This knowledge is crucial for the nanotechnology researchers and engineers to produce reliable designs of nano-scale devices and nanotechnology applications.

Keywords: Nanotechnology; Mechanistic model; Nanobeams/plates; Surface energy

Project title:(English) Mechanistic Model for Analysis of Nano-scale Beams and Rectangular Plates with Surface Stress Effects

(Thai) แบบจำลองทางกลศาสตร์สำหรับการวิเคราะห์คานและแผ่นพื้นสี่เหลี่ยมขนาดนาโนโดยคำนึงถึงอิทธิพลของหน่วยแรงที่ผิว

1. Abstract

(Thai) นาโนเทคโนโลยีเป็นเทคโนโลยีใหม่ที่สามารถประยุกต์ใช้งานได้หลากหลายเช่น ด้านคอมพิวเตอร์ อุปกรณ์อิเล็คโทรนิค และอุปกรณ์ทางการแพทย์ เป็นต้น การพัฒนานาโนเทคโนโลยีจำเป็นต้องอาศัยความเข้าใจพฤติกรรมการตอบสนองของโครงสร้างระดับนาโนประเภทต่างๆ เช่น คานขนาดนาโน ท่อนาโนคาร์บอน อนุภาคนาโนและแผ่นพื้นขนาดนาโน ซึ่งโครงสร้างระดับนาโนเหล่านี้เป็นส่วนประกอบที่สำคัญของอุปกรณ์ระดับนาโน งานวิจัยนี้ต้องการพัฒนาแบบจำลองทางทฤษฎีที่เหมาะสมสำหรับวิเคราะห์พฤติกรรมที่ซับซ้อนของคานขนาดนาโนและแผ่นพื้นสี่เหลี่ยมขนาดนาโน แบบจำลองทางกลศาสตร์สำหรับการวิเคราะห์คานและแผ่นพื้นสี่เหลี่ยมขนาดนาโนถูกพัฒนาโดยคำนึงถึงอิทธิพลของหน่วยแรงที่ผิว และนำไปใช้ศึกษาผลกระทบจากอิทธิพลของขนาดและขอบเขตเงื่อนไขต่อการตอบสนองของคานและแผ่นพื้นสี่เหลี่ยมขนาดนาโน ความรู้ที่ได้จากการศึกษานี้เป็นความรู้พื้นฐานที่สำคัญสำหรับนักวิจัยด้านนาโนเทคโนโลยี รวมถึงเป็นประโยชน์สำหรับการออกแบบอุปกรณ์ระดับนาโนและการประยุกต์ใช้นาโนเทคโนโลยี

คำสำคัญ: นาโนเทคโนโลยี แบบจำลองทางกลศาสตร์ คานและแผ่นพื้นขนาดนาโน หน่วยแรงที่ผิว

2. Executive Summary

Nanotechnology has remarkably become one of the most interesting fields of research and technology that offers a wide range of applications. For instance, researchers have developed a noninvasive surgery method that could blast tumors or other diseased areas without damaging healthy tissue by using a lens coated with carbon nanotubes to convert light from a laser to focused sound waves. Nanowires are being explored due to their unique chemical and electrical properties to make efficient solar cells. Nano-crystalline silicon carbide has been used in hard protective coatings for computer hard disks. For public utilities, researchers are developing economical and efficient water purification technique which would allow inhabitants in the third-world countries to access clean water. According to existing and potential benefits to various applications and a growing demand for high performance nano-scale devices, nanotechnology will undoubtedly become a frontier revolutionary technology capable of profoundly impacting our society.

Nano-scale beams and plates are the key components of nanoelectromechanical system (NEMS)-based technology and other nano-scale devices. To successfully design and manufacture nano-scale devices, a fundamental understanding of their mechanical properties and behavior is required. Investigation of nano-mechanical properties and responses can be achieved by either conducting experiments or performing mathematical simulations. For structures with nano-scale dimensions such as nanobeams and nanoplates which have relatively high surface area-to-volume ratio, the size effect due to surface energy can play an important role on their mechanical properties and responses. Nanobeam experiments, for instance, show a complex size-dependency of elastic modulus that is influenced by beam thickness and end boundary conditions. Mathematical simulations based on conventional concepts of mechanics, therefore, need to be modified to account for surface energy effects that exist at the nano-scale.

Based on the above introduction, it is clear that an understanding of size-dependent behavior of the structures at nano-scale is critical for an effective and reliable design of nano-scale devices and nanotechnology applications. Significant research efforts, therefore, need to be directed toward the investigation related to the mechanical responses of nano-scale structures. To serve these challenges, this research project examines the key research issues related to the mechanical

responses of nano-scale beams and plates. Mechanistic models of nano-scale beams and plates incorporating surface stress effects are developed and applied to investigate the influence of various parameters such as size effects and boundary conditions on responses of nanobeams and nanoplates. The outcomes from the present research provide a better understanding of mechanical responses of nanobeams and nanoplates, which are useful in the development and improvement of nano-scale devices and nanotechnology applications.

3. Objectives of the Research Project

The objectives of the research project are:

1) To develop mechanistic models incorporating surface effects based on Gurtin-Murdoch continuum theory for analysis of nano-scale beams by means of the principle of equilibrium.

2) To verify the governing equation and identify admissible boundary conditions of nano-scale beams by means of the variational formulation. In addition, analytical solutions for nano-scale beams with different end boundary conditions are to be re-derived and examined.

3) To employ the nano-scale beam model and solutions obtained from 1) and 2) to investigate the influence of size effect and end boundary conditions on the response of nanobeams.

4) To develop mechanistic models incorporating surface effects based on Gurtin-Murdoch continuum theory for static and dynamic analysis of nano-scale rectangular plates.

5) To construct analytical and finite element (FE) solutions for static and dynamic analysis of nano-scale rectangular plates.

6) To employ the nano-scale rectangular plate model and solutions obtained from 4) and 5) to investigate the influence of size effects and boundary conditions on static and dynamic responses of rectangular nanoplates.

4. Research methodology

The present research project is concerned with the development of mechanistic models incorporating surface stress effects for the analysis of nano-scale beams

and rectangular plates. The research methodology, procedures and fundamental theories to be employed in the research project are summarized as follows:

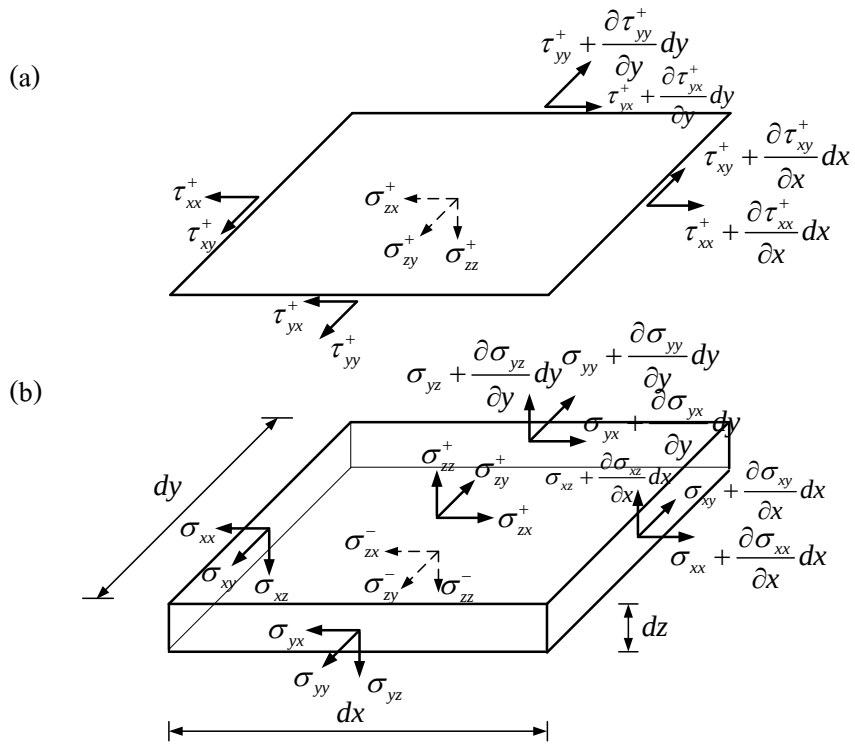

Figure 1 (a) Surface stresses on an incremental element of top surface layer; and (b) stress components of an incremental bulk element.

4.1 Development of nano-scale rectangular plate models

Consider an incremental element of a thin rectangular nanoplate with a Cartesian coordinate system (x, y, z) as shown in Fig.1. It is assumed that the response of the plate is governed by the continuum theory proposed by Gurtin and Murdoch (1975a, 1975b) and its deflections are small and strains are infinitesimal. According to the Gurtin-Murdoch theory (Gurtin and Murdoch, 1975a and 1975b), the plate element consists of a bulk material and surface layer of zero mathematical thickness. Stresses acting on the surface and bulk incremental elements are shown in Fig. 1(a) and Fig. 1(b) respectively. The elastic properties of surface element are surface Lamé constants λ_0 and μ_0, surface residual stress under unstrained conditions τ_0, and the surface mass density (defined as the mass of atoms of a unit

surface area) ρ_0. From Gurtin-Murdoch theory (Gurtin and Murdoch, 1975a and 1975b),

$$\tau_{\alpha\beta}^{\pm} = \tau_0\delta_{\alpha\beta} + (\mu_0 - \tau_0)\left(u_{\alpha,\beta}^{\pm} + u_{\beta,\alpha}^{\pm}\right) + (\tau_0 + \lambda_0)u_{\gamma,\gamma}^{\pm}\delta_{\alpha\beta} + \tau_0 u_{\alpha,\beta}^{\pm} \tag{1a}$$

$$\tau_{\alpha z}^{\pm} = \tau_0 u_{z,\alpha}^{\pm} \tag{1b}$$

where $\tau_{\alpha\beta}^{\pm}(\alpha,\beta = x,y)$ with superscripts ' + ' and ' – ' denotes the surface stress components of the top and bottom surfaces respectively.

The force equilibrium equations of the top (Fig. 1(a)) and bottom surfaces can be expressed as,

$$\tau_{\alpha i,\alpha}^{+} - \sigma_{zi}^{+} = \rho_0^{+}\ddot{u}_i^{+} \tag{2a}$$

$$\tau_{\alpha i,\alpha}^{-} + \sigma_{zi}^{-} = \rho_0^{-}\ddot{u}_i^{-} \tag{2b}$$

where σ_{zi}^{+} ($i = x,y,z$) is the resulting contact tractions existing on the interface of bulk and top surface layers due to the interaction between the surface layer and bulk.

Equilibrium of an incremental element of the bulk (Fig. 1(b)) in the $x-$direction can be expressed as:

$$\int_{-h/2}^{h/2}\frac{\partial\sigma_{xx}}{\partial x}dz + \int_{-h/2}^{h/2}\frac{\partial\sigma_{yx}}{\partial y}dz + \sigma_{zx}^{+} - \sigma_{zx}^{-} + \int_{-h/2}^{h/2} b_x dz = \int_{-h/2}^{h/2}\rho\ddot{u}_x dz \tag{3}$$

where σ_{ij}, b_i and ρ are bulk stresses, body forces and mass density of the bulk material respectively; and h is the thickness of the plate.

Similarly, the equilibrium of the bulk element in the y- and z-directions respectively yield,

$$\int_{-h/2}^{h/2}\frac{\partial\sigma_{xy}}{\partial x}dz + \int_{-h/2}^{h/2}\frac{\partial\sigma_{yy}}{\partial y}dz + \sigma_{zy}^{+} - \sigma_{zy}^{-} + \int_{-h/2}^{h/2} b_y dz = \int_{-h/2}^{h/2}\rho\ddot{u}_y dz \tag{4a}$$

$$\int_{-h/2}^{h/2}\frac{\partial\sigma_{xz}}{\partial x}dz + \int_{-h/2}^{h/2}\frac{\partial\sigma_{yz}}{\partial y}dz + \sigma_{zz}^{+} - \sigma_{zz}^{-} + \int_{-h/2}^{h/2} b_z dz + q(x,y) = \int_{-h/2}^{h/2}\rho\ddot{u}_z dz \tag{4b}$$

where $q(x,y)$ denotes the applied loading on the plate.

Next, the moment equilibrium equations of the bulk element about the y- and x-axis can be expressed as:

$$\int_{-h/2}^{h/2}\left(\frac{\partial\sigma_{xx}}{\partial x}+\frac{\partial\sigma_{yx}}{\partial y}\right)z dz+\frac{h}{2}\left(\sigma_{zx}^{+}+\sigma_{zx}^{-}\right)-\int_{-h/2}^{h/2}\sigma_{xz}\,dz+\int_{-h/2}^{h/2}b_x\,z dz=\int_{-h/2}^{h/2}\rho\ddot{u}_x\,z dz \qquad (5a)$$

and

$$\int_{-h/2}^{h/2}\left(\frac{\partial\sigma_{xy}}{\partial x}+\frac{\partial\sigma_{yy}}{\partial y}\right)z dz+\frac{h}{2}\left(\sigma_{zy}^{+}+\sigma_{zy}^{-}\right)-\int_{-h/2}^{h/2}\sigma_{yz}\,dz+\int_{-h/2}^{h/2}b_y\,z dz=\int_{-h/2}^{h/2}\rho\ddot{u}_y\,z dz \qquad (5b)$$

Assume that the bulk material is homogeneous and isotropic and let E and ν denote its Young's modulus and Poisson's ratio respectively. Its constitutive relations can be expressed as,

$$\sigma_{xx}=\frac{E}{1-\nu^2}\varepsilon_{xx}+\frac{E\nu}{1-\nu^2}\varepsilon_{yy}+\frac{\nu}{1-\nu}\sigma_{zz} \qquad (6a)$$

$$\sigma_{yy}=\frac{E}{1-\nu^2}\varepsilon_{yy}+\frac{E\nu}{1-\nu^2}\varepsilon_{xx}+\frac{\nu}{1-\nu}\sigma_{zz} \qquad (6b)$$

$$\sigma_{i\alpha}=\frac{E}{1-\nu^2}\varepsilon_{i\alpha} \qquad (6c)$$

In the present research project, bulk stress σ_{zz} is assumed to vary linearly through the plate thickness to satisfy the equilibrium conditions on the surface. Therefore,

$$\sigma_{zz}=\frac{1}{2}(\sigma_{zz}^{+}+\sigma_{zz}^{-})+\frac{z}{h}(\sigma_{zz}^{+}-\sigma_{zz}^{-}) \qquad (7)$$

Rewriting σ_{zz} in terms of surface stresses using Eq. (2) and assuming ρ_0^{+} = ρ_0^{-} = ρ_0 yields,

$$\sigma_{zz}=\frac{1}{2}(\tau_{\alpha z,\alpha}^{+}-\tau_{\alpha z,\alpha}^{-}-\rho_0\ddot{u}_z^{+}+\rho_0\ddot{u}_z^{-})+\frac{z}{h}(\tau_{\alpha z,\alpha}^{+}+\tau_{\alpha z,\alpha}^{-}-\rho_0\ddot{u}_z^{+}-\rho_0\ddot{u}_z^{-}) \qquad (8)$$

For a Kirchhoff plate,

$$u_x=-z\frac{\partial w}{\partial x};\ u_y=-z\frac{\partial w}{\partial y};\ u_z=w(x,y) \qquad (9)$$

where $w(x,y)$ denotes the vertical displacement of the plate.

The relevant strain-displacement relations for the bulk materials are,

$$\varepsilon_{xx} = -z\frac{\partial^2 w}{\partial x^2};\ \varepsilon_{yy} = -z\frac{\partial^2 w}{\partial y^2};\ \varepsilon_{xy} = -z\frac{\partial^2 w}{\partial x \partial y} \tag{10}$$

and $\varepsilon_{xz} = \varepsilon_{yz} = \varepsilon_{zz} = 0$.

After further manipulations, the following governing equation for a thin plate incorporating the effects of surface energy can be obtained based on Eqs. (1) - (10).

$$\begin{aligned} & D^*\left(\frac{\partial^4 w}{\partial x^4} + 2\frac{\partial^4 w}{\partial x^2 \partial y^2} + \frac{\partial^4 w}{\partial y^4}\right) - 2\tau_0\left(\frac{\partial^2 w}{\partial x^2} + \frac{\partial^2 w}{\partial y^2}\right) + q(x,y) \\ & = -(\rho h + 2\rho_0)\frac{\partial^2 w}{\partial t^2} + \left(\frac{\rho^3 h}{12} + \frac{\rho_0 h^2}{2} - \frac{\rho_0 h^2 \nu}{6(1-\nu)}\right)\left(\frac{\partial^4 w}{\partial x^2 \partial t^2} + \frac{\partial^4 w}{\partial y^2 \partial t^2}\right) \end{aligned} \tag{11}$$

where $D^* = \frac{Eh^3}{12(1-\nu^2)} + \frac{h^2}{2}(2\mu_0 + \lambda_0) - \frac{h^2 \tau_0 \nu}{6(1-\nu)}$.

4.2 Variational formulation of nano-scale beam model

Consider a thin beam with cross-section symmetric about the z-axis and length L as shown in Fig. 2. A beam based on the Gurtin-Murdoch continuum model has an elastic surface (mathematically zero thickness) perfectly bonded to the bulk material. The outward unit normal n and tangent t of the cross-section are as shown in Fig. 2. The elastic surface has distinct material properties and accounts for the surface energy effects (Miller and Shenoy, 2000; Lee and Rudd, 2007).

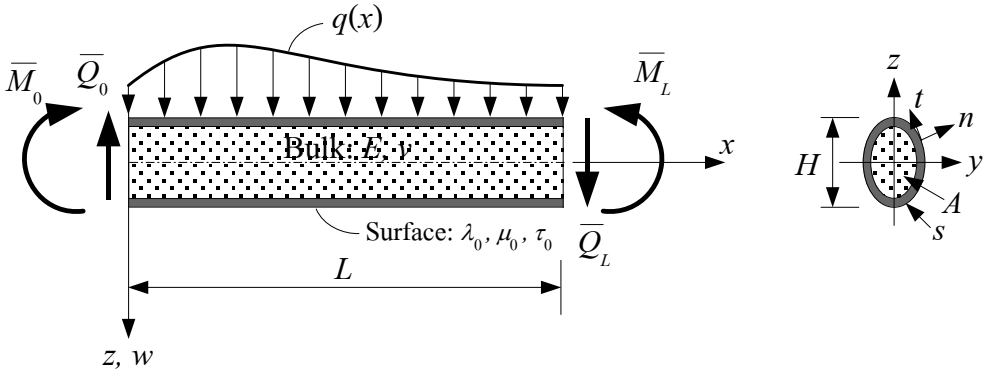

Figure 2 Geometry of beam and coordinate system.

Let w denote the deflection along the centroidal axis $(x,0,0)$ of the beam. For thin beams with Euler-Bernoulli hypothesis, the displacements u_x and u_z along the x- and z-directions are given by:

$$u_x = -z\frac{\partial w(x,t)}{\partial x}; \quad u_z = w(x,t) \tag{12}$$

Therefore, the non-zero bulk strain is:

$$\varepsilon_{xx} = \frac{\partial u_x}{\partial x} = -z\frac{\partial^2 w(x,t)}{\partial x^2} \tag{13}$$

The beam is in the plane stress state with non-zero bulk stresses, σ_{xx} and σ_{zz}. The elastic surface (outward unit normal n) has non-zero stresses τ_{xx} and τ_{nx}. Assuming a homogeneous and isotropic bulk material, the relevant constitutive relations of the bulk can be expressed as,

$$\sigma_{xx} = E\varepsilon_{xx} + \nu\sigma_{zz} \tag{14}$$

where E is the elastic modulus and ν is Poisson's ratio.

The stress component σ_{zz} is usually neglected in the classical beam theory. However, the Young-Laplace condition (Young, 1805; Laplace, 1805; Chen et al., 2006) along the surface- bulk interface requires a non-zero σ_{zz}. Following Lu et al. (2006), σ_{zz} is assumed to vary linearly through the beam thickness to satisfy the equilibrium conditions on the interface. Therefore,

$$\sigma_{zz} = \frac{1}{2}(\sigma_{zz}^{+} + \sigma_{zz}^{-}) + \frac{z}{H}(\sigma_{zz}^{+} - \sigma_{zz}^{-}) \tag{15}$$

where σ_{zz}^{+} and σ_{zz}^{-} are stresses at the top and bottom fibers, respectively, and H is the height of the beam.

The surface constitutive relations can be expressed as (Gurtin and Murdoch, 1975a and 1975b),

$$\tau_{xx} = \tau_0 + (2\mu_0 + \lambda_0)u_{x,x}; \quad \tau_{nx} = \tau_0 u_{n,x} \tag{16}$$

where τ_0 is the surface residual stress under unconstrained conditions; μ_0 and λ_0 are surface Lame constants; and u_x and u_n are the displacements along the x- and n-direction respectively.

The surface equilibrium at any point is expressed by (Gurtin and Murdoch, 1975a and 1975b),

$$\tau_{zx,x} - \sigma_{zz} n_z = \rho_0 \ddot{u}_z^s \tag{17}$$

where $\ddot{u}_z^s$ denotes the acceleration of surface layer in the z-direction.

By substituting Eqs. (12), (13) and (17) into Eqs. (14), (15) and (16), the following expressions for non-zero stresses are obtained.

$$\sigma_{zz} = \frac{2z}{H}(\tau_0 \frac{\partial^2 w}{\partial x^2} - \rho_0 \ddot{w}); \qquad \sigma_{xx} = -Ez\frac{\partial^2 w}{\partial x^2} + \frac{2\nu z}{H}\left(\tau_0 \frac{\partial^2 w}{\partial x^2} - \rho_0 \ddot{w}\right) \tag{18}$$

$$\tau_{xx} = \tau_0 - z(2\mu_0 + \lambda_0)\frac{\partial^2 w}{\partial x^2}; \qquad \tau_{nx} = \tau_0 \frac{\partial w}{\partial x} n_z \tag{19}$$

The total strain energy of the beam contains two parts, i.e., the elastic strain energy stored in the bulk material (U^B) and the elastic strain energy of the surface (U^s):

$$U^B = \frac{1}{2}\int_V \sigma_{xx}\varepsilon_{xx} dV \;\; ; \;\; U^s = \frac{1}{2}\int_\Gamma (\tau_{xx}\varepsilon_{xx} + \tau_{nx}\varepsilon_{nx}) d\Gamma \tag{20}$$

where V is the bulk volume and Γ is the surface area.

From Eqs. (18), (19) and (20), the strain energies stored in the bulk and surface can be expressed as,

$$U^B = \frac{1}{2}\left(EI - \frac{2\nu I \tau_0}{H}\right)\int_0^L \left(\frac{\partial^2 w}{\partial x^2}\right)^2 dx + \frac{2\nu I \rho_0}{H}\int_0^L \ddot{w}\left(\frac{\partial^2 w}{\partial x^2}\right) dx \tag{21}$$

$$U^s = \frac{1}{2}(2\mu_0 + \lambda_0) I^* \int_0^L \left(\frac{\partial^2 w}{\partial x^2}\right)^2 dx + \frac{1}{2}\tau_0 s^* \int_0^L \left(\frac{\partial w}{\partial x}\right)^2 dx \tag{22}$$

where $I = \int_A z^2 dA$ is the moment of inertia of the beam cross-section; $I^* = \int_s z^2 ds$ is the perimeter moment of inertia; $s^* = \int_s n_z^2 ds$; A is the cross-sectional area and s is the perimeter of the cross section.

In the case of beams with rectangular cross-section of height $2h$ and width b, the geometry parameters are given as,

$$I = \frac{2bh^3}{3}; \;\; I^* = 2bh^2 + \frac{4h^3}{3}; \; s^* = 2b \text{ and } H = 2h \tag{23}$$

The potential energy due to a distributed load $q(x)$ on the beam, prescribed end moment ($\bar{M}$) and end force ($\bar{Q}$), as shown in Fig. 2, is

$$V = -\int_0^L q(x)w(x)dx + \left(\bar{M}\frac{\partial w}{\partial x}\right)\Big|_0^L - \left(\bar{Q}w\right)\Big|_0^L \tag{24}$$

where $\bar{M}$ and $\bar{Q}$ are the moment and force at the ends of the beam respectively.

The kinetic energy of nanoscale beam is,

$$T = \frac{1}{2}\int_0^L \rho A(\dot{w})^2 dx + \frac{1}{2}\int_0^L \rho_0 s^*(\dot{w})^2 dx \tag{25}$$

In view of Eqs. (21), (22), (24) and (25), the total energy functional of nanoscale beam is,

$$\begin{aligned}\Pi(x,w,w',w'') &= U^B + U^s + V + T \\ &= \frac{1}{2}\left[EI - \frac{2\nu I\tau_0}{H} + (2\mu_0+\lambda_0)I^*\right]\int_0^L\left(\frac{\partial^2 w}{\partial x^2}\right)^2 dx + \frac{1}{2}\tau_0 s^*\int_0^L\left(\frac{\partial w}{\partial x}\right)^2 dx \\ &\quad + \frac{2\nu I\rho_0}{H}\int_0^L \ddot{w}\left(\frac{\partial^2 w}{\partial x^2}\right)dx + \frac{1}{2}\int_0^L \rho A(\dot{w})^2 dx + \frac{1}{2}\int_0^L \rho_0 s^*(\dot{w})^2 dx \\ &\quad - \int_0^L q(x)w(x)dx + \left(\bar{M}\frac{\partial w}{\partial x}\right)\Big|_0^L - \left(\bar{Q}w\right)\Big|_0^L \end{aligned} \tag{26}$$

Taking the variation of Eq. (26) together with integration by parts leads to the following governing equation for a beam (Washizu, 1982):

$$\left[EI - \frac{2\nu I\tau_0}{H} + (2\mu_0+\lambda_0)I^*\right]\frac{\partial^4 w}{\partial x^4} - \tau_0 s^*\frac{\partial^2 w}{\partial x^2} - q$$

$$= -\frac{2\nu I\rho_0}{H}\frac{\partial^4 w}{\partial x^2\partial t^2} - (\rho A + \rho_0 s^*)\frac{\partial^2 w}{\partial t^2}, \qquad 0 < x < L \tag{27}$$

and the admissible boundary conditions for a nanoscale beam are:

$$\bar{Q} = -\left[EI - \frac{2\nu I\tau_0}{H} + (2\mu_0+\lambda_0)I^*\right]\left(\frac{\partial^3 w}{\partial x^3}\right) + \tau_0 s^*\frac{\partial w}{\partial x} - \frac{2\nu I\rho_0}{H}\frac{\partial^3 w}{\partial x\partial t^2} \quad \text{or} \quad w = \bar{w} \tag{28}$$

$$\bar{M} = -\left[EI - \frac{2\nu I\tau_0}{H} + (2\mu_0+\lambda_0)I^*\right]\left(\frac{\partial^2 w}{\partial x^2}\right) - \frac{2\nu I\rho_0}{H}\frac{\partial^2 w}{\partial t^2} \quad \text{or} \quad \frac{\partial w}{\partial x} = \bar{w}' \tag{29}$$

where $\bar{w}$ and $\bar{w}'$ denote the prescribed displacement and slope at the beam end respectively.

Equation (27) is similar to the classical beam equation but includes an additional term due to the effect of residual surface stress. It reduces to the classical model (Gere and Timoshenko, 1991) if the surface energy effect is completely neglected, i.e., μ_0, λ_0 and τ_0 are zero. Equations (27) - (29) are identical to the corresponding equations derived by Liu and Rajapakse (2010) using the force and moment equilibrium of an infinitesimal beam element. Based on Eq. (27), the modified bending stiffness of nanobeam can be defined as,

$$K_b^* = EI - \frac{2\nu I \tau_0}{H} + (2\mu_0 + \lambda_0) I^* \tag{30}$$

The homogeneous solution of Eq. (27) can be written as,

$$w(x) = C_1 e^{\sqrt{\varepsilon} x} + C_2 e^{-\sqrt{\varepsilon} x} + C_3 x + C_4 \tag{31}$$

where $\varepsilon = \tau_0 s^* / K_b^*$; K_b^* is defined by eq (19); and C_1 to C_4 are unknown arbitrary constants to be determined from the boundary conditions.

Details on the formulation of the analytical solutions including the explicit expression for static and free vibration of nanoscale rectangular plates under various boundary conditions are given by Sapsathiarn and Rajapakse (2016).

4.3 Finite element model of nano-scale rectangular plate

The finite element model of nano-scale rectangular plate provides an efficient tool to analyze and predict the mechanical response of plate elements encountered in nano-scale devices and other nanoelectromechanical systems. A finite element formulation of a nano-scale rectangular plate based on the Gurtin–Murdoch model (static and dynamic conditions) has been developed based on a weighted residual formulation. The governing equations for Gurtin-Murdoch nano-scale rectangular plate model are employed in the weighted residual FE formulation to explicitly obtain the plate stiffness and mass matrices.

Galerkin's weighted residual method is applied to Eq. (11) to develop the finite-element (FE) formulation for plates. Following Zienkiewicz and Taylor (2000), the weighted residual statement for static loading is:

$$\int_V \bar{w}\left\{D^*\left(\frac{\partial^4 w}{\partial x^4}+2\frac{\partial^4 w}{\partial x^2\partial y^2}+\frac{\partial^4 w}{\partial y^4}\right)-2\tau_0\left(\frac{\partial^2 w}{\partial x^2}+\frac{\partial^2 w}{\partial y^2}\right)+q(x,y)\right\}dV=0 \tag{32}$$

where V denote the volume of the plate and $\bar{w}$ is the weight function.

Integrating Eq. (32) by parts, the weak formulation can be written as,

$$\iint_{\Omega_0}\left\{D^*\frac{\partial^2\bar{w}}{\partial x^2}\left(\frac{\partial^2 w}{\partial x^2}+\nu\frac{\partial^2 w}{\partial y^2}\right)+D^*\frac{\partial^2\bar{w}}{\partial y^2}\left(\frac{\partial^2 w}{\partial y^2}+\nu\frac{\partial^2 w}{\partial x^2}\right)\right.$$
$$\left.+2(1-\nu)D^*\left(\frac{\partial^2\bar{w}}{\partial x\partial y}\frac{\partial^2 w}{\partial x\partial y}\right)+2\tau_0\left(\frac{\partial\bar{w}}{\partial x}\frac{\partial w}{\partial x}+\frac{\partial\bar{w}}{\partial y}\frac{\partial w}{\partial y}\right)+\bar{w}q\right\}dxdy=0 \tag{33}$$

A 4-node rectangular finite element with w, θ_x $[=\partial w/\partial x]$ and θ_y $[=\partial w/\partial y]$ as the nodal variables is considered. The element nodal displacement vector can be written as,

$$\{w^e\}=\begin{bmatrix} w^1 & \theta_x^1 & \theta_y^1 & \dots & w^4 & \theta_x^4 & \theta_y^4 \end{bmatrix}^{\mathrm{T}} \tag{34}$$

Vertical displacement, w, is interpolated by using a set of shape functions as,

$$w=\mathbf{N}\mathbf{w}^e=N_{11}w^1+N_{12}\theta_x^1+N_{13}\theta_y^1+\dots+N_{41}w^4+N_{42}\theta_x^4+N_{43}\theta_y^4 \tag{35}$$

where,

$$N_{i1}=\frac{1}{8}(1+\xi_0)(1+\eta_0)(2+\xi_0+\eta_0-\xi^2-\eta^2) \tag{36}$$

$$N_{i2}=\frac{1}{8}\xi_i(\xi_0-1)(1+\eta_0)(1+\xi_0)^2 \tag{37}$$

$$N_{i3}=\frac{1}{8}\eta_i(\eta_0-1)(1+\eta_0)(1+\eta_0)^2 \tag{38}$$

$$\xi=\frac{x-x_0}{a};\ \eta=\frac{y-y_0}{b};\ \xi_0=\xi\xi_i;\ \eta_0=\eta\eta_i \tag{39}$$

in which (x_0,y_0) are the global coordinates of the center of a rectangular plate finite element.

Substitution of Eq. (35) into Eq. (33), yields the element stiffness matrix ($\mathbf{K}^e$) and nodal force vector ($\mathbf{f}^e$) as,

$$\mathbf{K}^e=\int_{\Omega_0}\left\{\mathbf{B}_2{}^T\mathbf{C}\mathbf{B}_2+2\tau_0\mathbf{B}_1{}^T\mathbf{B}_1\right\}dxdy\ ;\ \mathbf{f}^e=\int_{\Omega_0}\mathbf{N}q\,dxdy \tag{40}$$

where,

$$\mathbf{B}_1 = \begin{bmatrix} \frac{\partial N_{11}}{\partial x} & \frac{\partial N_{12}}{\partial x} & \frac{\partial N_{13}}{\partial x} & \cdots & \frac{\partial N_{41}}{\partial x} & \frac{\partial N_{42}}{\partial x} & \frac{\partial N_{43}}{\partial x} \\ \frac{\partial N_{11}}{\partial y} & \frac{\partial N_{12}}{\partial y} & \frac{\partial N_{13}}{\partial y} & \cdots & \frac{\partial N_{41}}{\partial y} & \frac{\partial N_{42}}{\partial y} & \frac{\partial N_{43}}{\partial y} \end{bmatrix} \tag{41}$$

$$\mathbf{B}_2 = \begin{bmatrix} \frac{\partial^2 N_{11}}{\partial x^2} & \frac{\partial^2 N_{12}}{\partial x^2} & \frac{\partial^2 N_{13}}{\partial x^2} & \cdots & \frac{\partial^2 N_{41}}{\partial x^2} & \frac{\partial^2 N_{42}}{\partial x^2} & \frac{\partial^2 N_{43}}{\partial x^2} \\ \frac{\partial^2 N_{11}}{\partial y^2} & \frac{\partial^2 N_{12}}{\partial y^2} & \frac{\partial^2 N_{13}}{\partial y^2} & \cdots & \frac{\partial^2 N_{41}}{\partial y^2} & \frac{\partial^2 N_{42}}{\partial y^2} & \frac{\partial^2 N_{43}}{\partial y^2} \\ 2\frac{\partial^2 N_{11}}{\partial x \partial y} & 2\frac{\partial^2 N_{12}}{\partial x \partial y} & 2\frac{\partial^2 N_{13}}{\partial x \partial y} & \cdots & 2\frac{\partial^2 N_{41}}{\partial x \partial y} & 2\frac{\partial^2 N_{42}}{\partial x \partial y} & 2\frac{\partial^2 N_{43}}{\partial x \partial y} \end{bmatrix} \tag{42}$$

$$\mathbf{C} = \begin{bmatrix} D^* & \nu D^* & 0 \\ \nu D^* & D^* & 0 \\ 0 & 0 & \frac{(1-\nu)D^*}{2} \end{bmatrix} \tag{43}$$

It can be seen from Eq. (40) that surface stresses contribute to the stiffness matrix of a plate element. In the absence of surface stress effects, the stiffness matrix reduces to the classical elasticity case. The assembly of element stiffness matrices and nodal force vectors yields the following global equilibrium equation:

$$\mathbf{K}\mathbf{r} = \mathbf{f} \tag{44}$$

where $\mathbf{K}$, $\mathbf{r}$ and $\mathbf{f}$ are the global stiffness matrix, global nodal force vector and global generalized displacement vector, respectively.

For dynamic analysis, the inertia terms on the right hand side of Eq. (11) have to be considered in the finite element formulation, and these terms correspond to the element mass matrix. It can be shown that the element mass matrix is given by,

$$\mathbf{M}^e = \int_{\Omega_0} \left\{ (\rho h + 2\rho_0)\mathbf{N}^T\mathbf{N} + \left(\frac{\rho^3 h}{12} + \frac{\rho_0 h^2}{2} - \frac{\rho_0 h^2 \nu}{6(1-\nu)} \right) \mathbf{B}_1{}^T \mathbf{B}_1 \right\} dxdy \tag{45}$$

The global finite element equation for dynamic analysis is:

$$\mathbf{M}\ddot{\mathbf{r}} + \mathbf{K}\mathbf{r} = \mathbf{f} \tag{46}$$

where $\mathbf{M}$ is the global mass matrix.

Substituting $\mathbf{r}(t) = e^{i\omega t}\mathbf{r}$ in Eq. (46), the natural frequencies and mode shapes can be obtained by solving the following eigenvalue problem.

$$\left[\mathbf{K} - \omega^2 \mathbf{M}\right]\mathbf{r} = \mathbf{0} \tag{47}$$

where ω is the frequency of vibration in rad/s.

5. Results and Discussion

5.1 Nano-scale rectangular plate

A comparison of the finite element model for plate static deflections and natural frequencies with the analytical results available in literature is presented for the case of elastic rectangular plate without surface effects. A plate with all edges simply supported (SSSS) under uniformly distributed loading is considered. Due the symmetry of the plate geometry and loading, a quarter model with $N \times N$ elements is employed for the finite element analysis.

Table 1 Comparison of deflections of simply-supported (SSSS) plates under uniformly distributed load (a = 200 nm, b = 200 nm, h = 10 nm).

Material		FE solution (Quarter model)				Analytical
		2×2	4×4	10×10	12×12	Solution
Al	*w*(0,0)	0.03864	0.03735	0.03698	0.03696	0.03690
		(0.04902)	(0.04689)	(0.04628)	(0.04625)	(0.04617)
	w(0.25*a*,0.25*a*)	0.02811	0.02715	0.02688	0.02687	0.02683
		(0.03546)	(0.03392)	(0.03348)	(0.03345)	(0.03339)
Si	*w*(0,0)	0.03810	0.03667	0.03627	0.03625	0.03619
		(0.04636)	(0.04418)	(0.04357)	(0.04353)	(0.04344)
	w(0.25*a*,0.25*a*)	0.02769	0.02665	0.02635	0.02633	0.02629
		(0.03354)	(0.03196)	(0.03151)	(0.03148)	(0.03142)

Deflections corresponding to the classical plate theory are shown in parenthesis.

The numerical results for both finite element solutions and analytical solutions are presented in Table 1. The finite element solutions converge and agree within 0.3% of analytical solutions when the number of plate elements, $N \geq 10$. Accuracy of the present solution is also verified by comparing with the limiting case of classical plate theory solutions (Timoshenko and Woinowsky, 1959). The solutions from current model are obtained for the classical case by setting the surface

material coefficients μ_0, λ_0 and τ_0 to zero. These comparisons are not presented in the report for brevity. Very good agreement between the two sets of solutions is noted.

Next, selected numerical results are presented to investigate the influence of surface properties and boundary conditions on the size-dependent static and free vibration response. Plates made of aluminum (Al) and silicon (Si) are used in the numerical study. The relevant bulk and surface material properties are given in Table 2 (Miller and Shenoy, 2000; Shenoy, 2005).

Table 2 Material properties of aluminum and silicon.

Material	E (GPa)	ν	μ_0 (N/m)	λ_0 (N/m)	τ_0 (N/m)	ρ (kg/m^3)	ρ_0 (kg/m^2)
Al	90	0.23	-0.54251	3.4939	0.5689	2.7×10^{3}	5.46×10^{-7}
Si	107	0.33	-2.7779	-4.4939	0.6056	2.33×10^{3}	3.17×10^{-7}

Deflection profiles of Si and Al nanoplates with all edges simply-supported (SSSS) under a uniformly distributed load (q_0) and a concentrated point load (P_0) at the center of the plate are shown in Fig. 3 and Fig. 4 respectively. Non-dimensional central displacement of the plate, w_q = $w(0,0)Eh^3/(q_0 a^4)$ and w_P = $w(0,0)Eh^3/(P_0 a^2)$ are considered in the numerical study. The solutions for an identical classical plate (zero surface material parameters) (Timoshenko and Woinowsky, 1959) are also shown in Figs. 3 and 4 for comparison. These numerical results clearly show that surface energy effects have a significant influence on plate deflections. It is observed that static deflections of Al and Si nanoplates under both types of loading are lower than the corresponding classical plate solutions. This implies that surface energy effects make the plates stiffer compared to the classical plate theory.

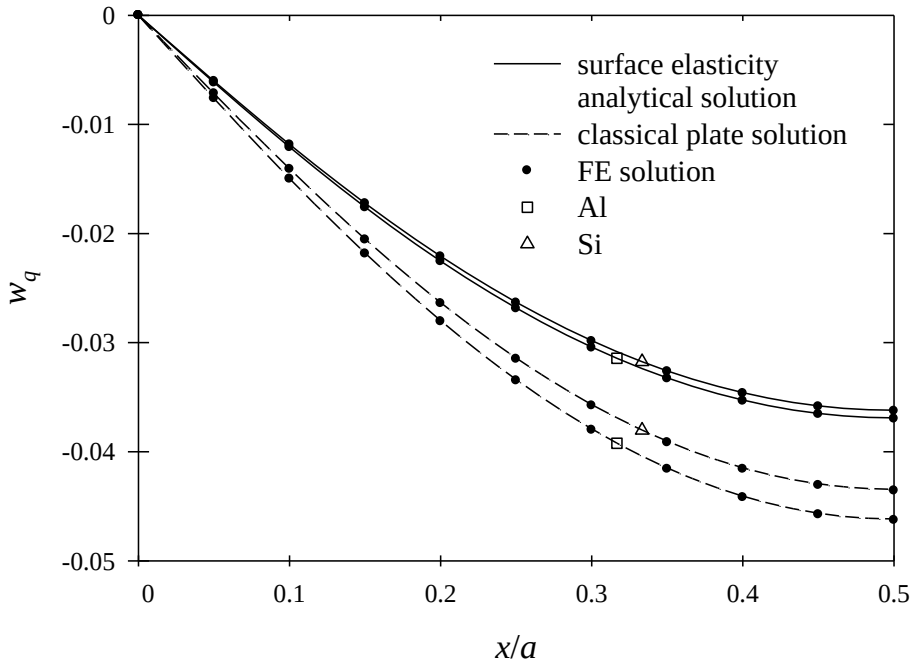

Figure 3 Deflection profiles of Al and Si plates with all edges simply-supported (SSSS) under uniformly distributed load (a = 200 nm, b = 200 nm, h = 10 nm).

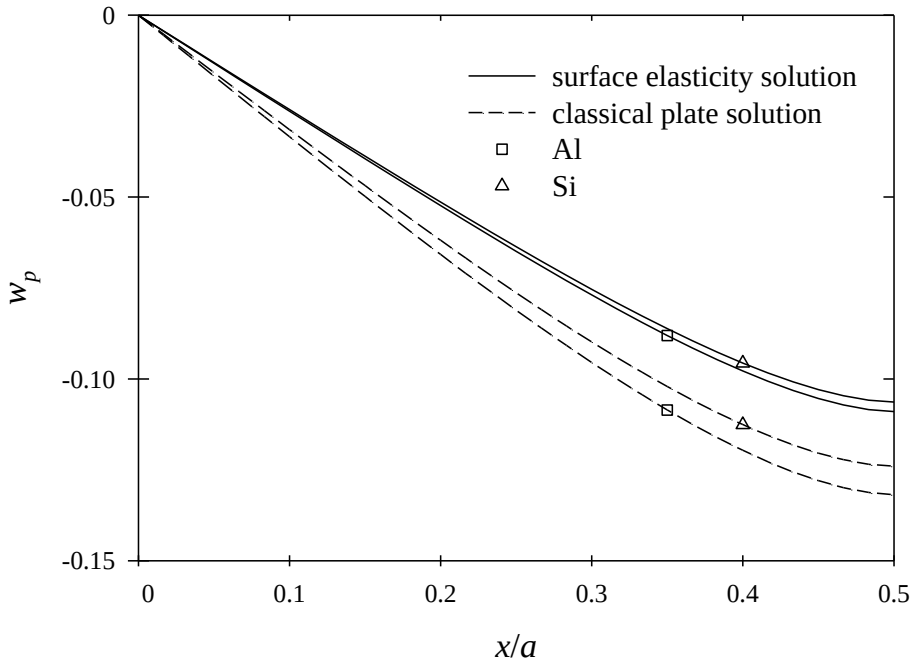

Figure 4 Deflection profiles of Al and Si plates with all edges simply-supported (SSSS) under point load (a = 200 nm, b = 200 nm, h = 10 nm).

Deflection profiles of Al and Si plates with two opposite edges simply supported and other two edges clamped (SCSC) and plates with all edges clamped (CCCC) are shown in Figs. 5 and 6 respectively. Similar to a simply-supported plate (Fig. 3), surface energy effects produces stiffening of plates but the effect is less prominent. Note that the main contribution from the surface energy is due to the surface residual stress τ_0 and the associated Young-Laplace effect that is directly proportional to the plate curvature. The radius of curvature of a plate with clamped edges is generally higher than a simply supported plate. Therefore the influence of surface residual stress is more prominent for simply supported plates. Similar behavior was also observed for nanobeams (Liu and Rajapakse, 2010).

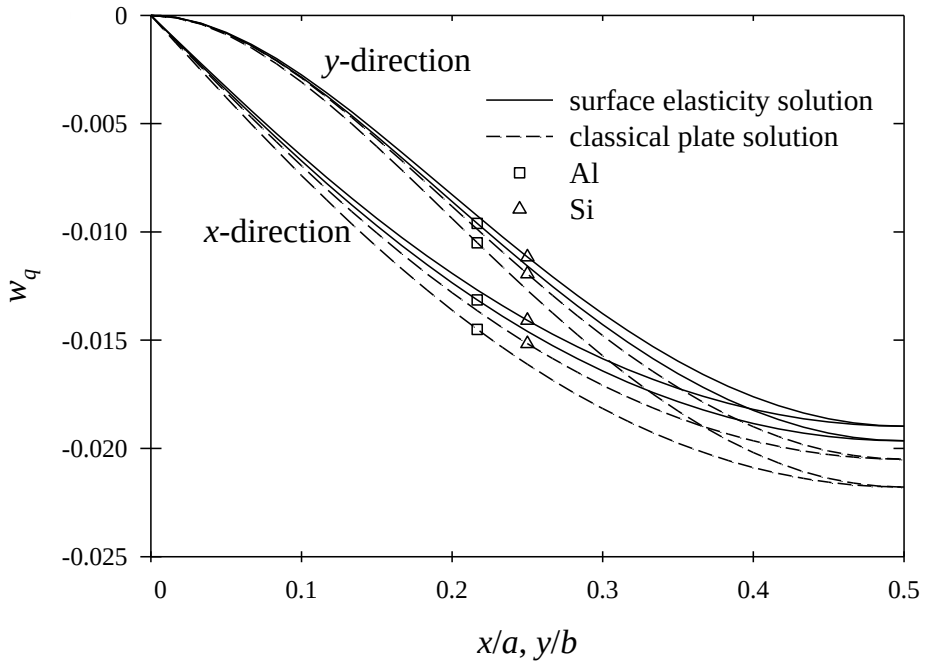

Figure 5 Deflection profiles of silicon SCSC plates under uniformly distributed load (a = 200 nm, b = 200 nm, h = 10 nm).

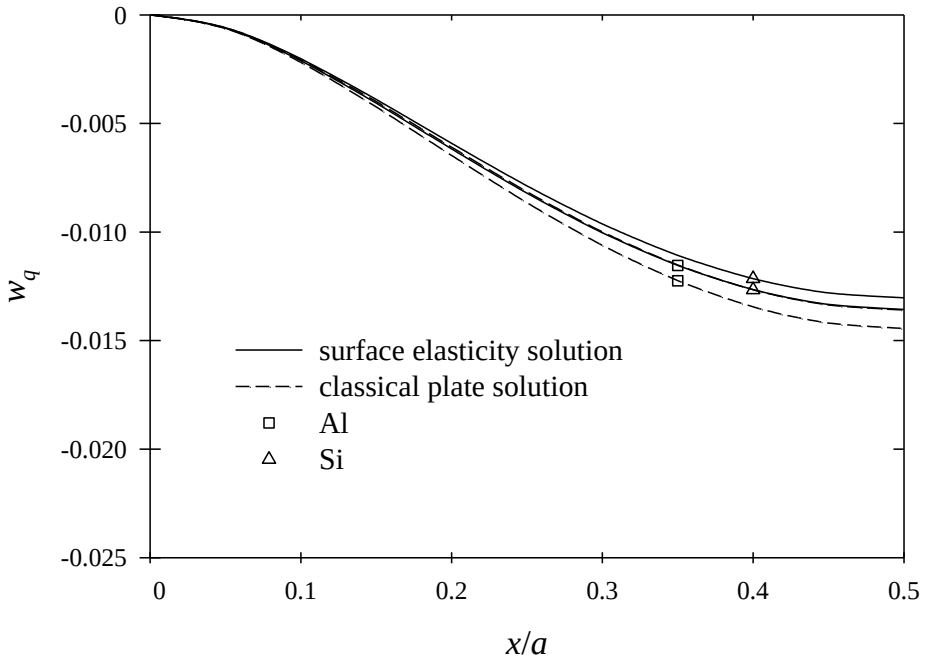

Figure 6 Deflection profiles of Al and Si plates with all edges clamped (CCCC) under uniformly distributed load (a = 200 nm, b = 200 nm, h = 10 nm).

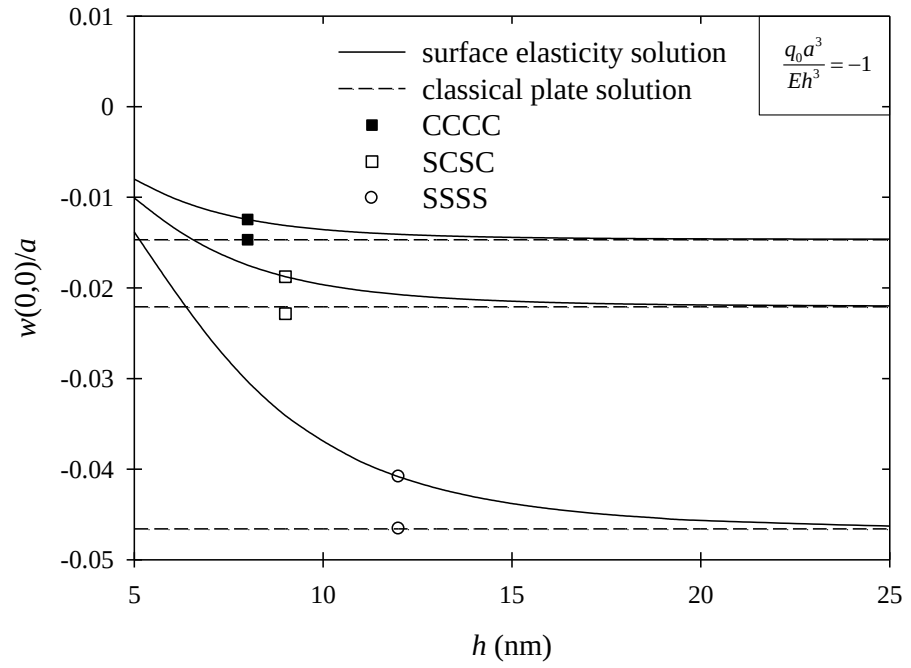

Figure 7 Size-effect of central deflection of uniformly loaded Al plates with different thicknesses under SSSS, SCSC and CCCC boundary conditions (a = 200 nm, b = 200 nm).

Size-effect of the response of nanoplates subjected to a uniformly distributed load (q_0) for different boundary conditions is illustrated in Fig. 7. Plates made of aluminum (Al) with a = 200 nm, b = 200 nm and thickness (h) varying from 5 – 25 nm are considered. Variation of normalized plate deflection, $w(0,0)/a$, where $w(0,0)$ is the deflection at the center of the plate with the plate thickness is plotted in Fig. 7 in which the nondimensional applied load is kept constant for all plates, i.e., $q_0 a^3/(Eh^3)$ = -1. The classical solutions for the three boundary conditions are identical and independent of plate thickness for a given nondimensional loading and plate boundary conditions. The size-effect on the normalized deflection compared to the classical case is clearly evident from Fig. 7 and the solutions confirm that the plate behavior significantly depends on the presence of surface residual stress. In addition, the size-dependency of the plate response depends on the boundary conditions of the plate. Plates with all edges simply-supported (SSSS) show the highest dependency on size followed by SCSC plates and clamped plates (CCCC). Furthermore, the numerical results reveal that the size-effects reduce with increasing plate thickness h. In particular, size-dependent behavior becomes negligible when the thickness of the plate is greater than 20 nm.

Table 3 Natural frequencies of Al and Si nanoplates for different boundary conditions (a = 200 nm, b = 200 nm, h = 10 nm).

Material	Boundary condition	Natural frequency (GHz)			
		ω_{11}	ω_{22}	ω_{33}	ω_{44}
Al	SSSS	9.242	33.569	74.027	130.656
		(8.451)	(33.805)	(76.061)	(135.220)
	SCSC	13.200	40.452	85.203	135.449
		(12.567)	(40.294)	(86.056)	(137.666)
	CCCC	16.072	45.932	89.540	144.146
		(15.614)	(45.991)	(90.602)	(146.534)
Si	SSSS	11.028	40.574	89.740	158.561
		(10.227)	(40.906)	(92.039)	(163.630)
	SCSC	15.773	48.602	102.503	163.170
		(15.205)	(48.707)	(103.946)	(166.356)
	CCCC	19.258	55.221	107.664	173.122
		(18.890)	(55.578)	(109.331)	(176.504)

Natural frequency from the corresponding classical plate theory is shown in parenthesis.

Natural frequencies of Al and Si nanoplates with different boundary conditions, i.e., SSSS, SCSC and CCCC, are presented in Table 3. It is noted that plate mode shapes are not significantly altered from the corresponding classical plate mode shapes. Natural frequencies obtained from the classical plate theory for identical plates are shown in parenthesis in Table 3. Table 3 confirms that the surface stress plays an important role on the first (lowest) natural frequency of both Al and Si nanoplates. The effect is more prominent in the case of simply supported boundary conditions (SSSS) when compared to the cases of CCCC and SCSC plates, similar to the behavior observed for deflection profiles. Presence of surface stresses leads to higher fundamental natural frequencies for all types of boundary conditions when compared to the corresponding classical plates. This behavior is also consistent with the stiffer response of nanoplates observed in Figs. 3-5. It is also observed that the surface effect is less significant on higher natural frequencies while the classical plate solutions for higher modes are slightly larger than the corresponding nanoplate solutions.

5.2 Nano-scale beam

5.2.1 Examination of the discrepancy between existing solutions

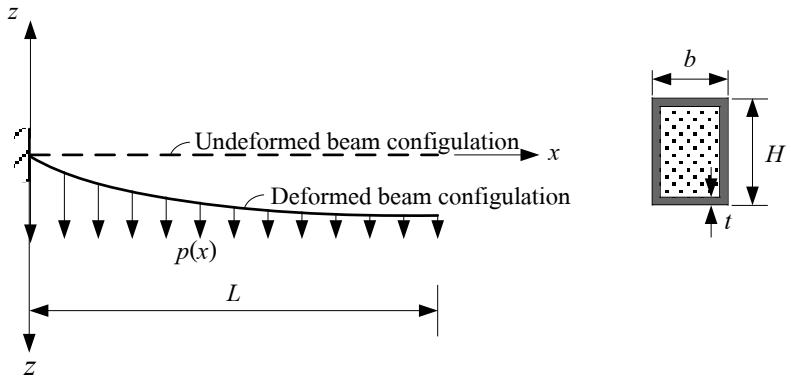

Figure 8 Nanobeam model of He and Lilley (2008).

Consider the solution developed by He and Lilley (2008) for the beam shown in Fig. 8. They derived the governing equation by simply adding an equivalent distributed loading due to surface residual stress (Young-Laplace effect) to the classical beam equation with a modified beam stiffness. Their governing equation is,

$$K_b^{**}\frac{d^4w}{dx^4} = p(x) \tag{48}$$

and in the absence of any applied distributed loading, $p(x)$ was defined by He and Lilley (2008) as

$$p(x) = 2(\tau_0 + E_s \varepsilon_x) b \frac{d^2 w}{dx^2} \tag{49}$$

where E_s is the surface elastic modulus, ε_x is the longitudinal surface strain and *b* is the beam width.

The modified bending stiffness of a rectangular beam K_b^{**} was determined by adding the stiffness contributions of surface layer with thickness *t* and bulk material (Fig. 8). Assuming $t \ll H$, He and Lilley (2008) expressed the stiffness of nanoscale beam by

$$K_b^{**} = EI_1 + \frac{1}{2} E_s b H^2 + \frac{1}{6} E_s H^3 \tag{50}$$

where $I_1 = \frac{1}{12} bH^3$.

By neglecting the contribution due to longitudinal surface strain in $p(x)$, the beam governing equation (48) was simplified to:

$$K_b^{**} \frac{d^4 w}{dx^4} \cong 2\tau_0 b \frac{d^2 w}{dx^2} \tag{51}$$

which can be re-written as

$$\left[EI + \frac{1}{2} E_s b H^2 + \frac{1}{6} E_s H^3 \right] \frac{d^4 w}{dx^4} - \tau_0 s^* \frac{d^2 w}{dx^2} = 0 \tag{52}$$

where $s^* = 2b$.

The above governing equation derived by He and Lilley (2008) is similar to the (static) results of Liu and Rajapakse (2010) and the present variational approach (see eq (16)), except that the modified beam stiffness is different. He and Lilley (2008) obtained the modified bending stiffness by simply adding the contribution of classical bending stiffness of the bulk and that due to a surface layer with finite thickness. However, the nanobeam stiffness given in the present formulation and Liu and Rajapakse (2010) are obtained based on the consideration of full elastic field based on the continuum model of Gurtin-Murdoch. Moreover, to satisfy the Gurtin-Murdoch surface equilibrium equations, the vertical bulk stress was also considered

by Liu and Rajapakse (2010) and in the present formulation. The influence of bulk vertical stress on the bending stiffness is represented by the second term of Eq. (27).

The homogeneous solutions of the governing equation of He and Lilley (2008) is also given by Eq. (31) with K_b^* (Eq. 30)) replaced by K_b^{**} (Eq. 50)). In the ensuing sections, beams under different end conditions, i.e., simply-supported, cantilevered, and clamped-clamped, are re-examined to identify the reason for the discrepancy between the Liu and Rajapakse (2010) and He and Lilley (2008).

5.2.2 Beams under different end conditions

5.2.2.1 Cantilever beams

Consider a cantilever beam of length L subjected to a concentrated static load $\bar{F}_L$ at the free end. According to the present scheme and Liu and Rajapakse (2010), Eq. (27) governs the (static response) beam and the boundary conditions are expressed by Eqs. (28) and (29) (by removing the dynamic term). Table 4 compares the boundary conditions used by Liu and Rajapakse (2010) and those used by He and Lilley (2008).

Table 4 Comparison of boundary conditions for cantilever beams.

Liu and Rajapakse (2010)	He and Lilley (2008)
1) $w(0) = 0$	1) $w(0) = 0$
2) $w'(0) = 0$	2) $w'(0) = 0$
3) $M^*(L) = 0$	3) Moment equilibrium at $x = 0$
4) $Q^*(L) = \bar{F}_L$	4) Vertical force equilibrium at $x = 0$

For a static problem, Eq. (27) is simplified to

$$K_b^* \frac{d^4 w}{dx^4} - \tau_0 s^* \frac{d^2 w}{dx^2} - q = 0 \tag{53}$$

and the corresponding natural boundary conditions are

$$\bar{Q} = -K_b^* \frac{d^3 w}{dx^3} + \tau_0 s^* \frac{dw}{dx} \quad \text{and} \quad \bar{M} = -K_b^* \frac{d^2 w}{dx^2} \tag{54}$$

The first and second boundary conditions are identical between the two models (see Table 4). In view of Eqs. (28) and (29), the third and fourth boundary conditions given by Liu and Rajapakse (2010) yield,

$$K_b^* w''(L) = 0 \quad \text{and} \quad -K_b^* w'''(L) + \tau_0 s^* w'(L) = \bar{F}_L \tag{55}$$

Using the first two boundary conditions of Table 4 and Eq. (55), the solution for cantilever beam can be obtained as,

$$w(x) = \frac{\bar{F}_L}{K_b^* \varepsilon}\left[x - \frac{\sinh(x\sqrt{\varepsilon} - L\sqrt{\varepsilon}) + \sinh(L\sqrt{\varepsilon})}{\sqrt{\varepsilon}\cosh(L\sqrt{\varepsilon})} \right] = \Omega f(x) \tag{56}$$

where Ω is a constant that depends on the magnitude of load, beam bending stiffness and surface residual stress; and $f(x)$ is a deflection shape function.

Instead of using boundary conditions at the beam ends to determine nanobeam solutions, He and Lilley (2008) replaced the third and the forth boundary conditions by the moment and force equilibrium conditions at $x = 0$ (see Table 4). Using the resultant shear force and bending moment of a nanobeam cross section defined in Eqs. (28) and (29) together with the condition of zero slope at $x = 0$, the moment and vertical force equilibrium at $x = 0$ can be written as

$$-K_b^{**} w''(0) = -\bar{F}_L L \quad \text{and} \quad -K_b^{**} w'''(0) = \bar{F}_L \tag{57}$$

The moment equilibrium condition at the beam end (x = 0) in Table 4 was, however, expressed by He and Lilley (2008) as,

$$K_b^{**} w''(0) = \bar{F}_L L + \int_0^L \tau_0 s^* w'' x\, dx = \bar{F}_L L + \tau_0 s^* \left[L w'(L) - w(L) \right] \tag{58}$$

and the force equilibrium at $x = 0$ was given by He and Lilley (2008) as,

$$-K_b^{**} w'''(0) = \bar{F}_L + \int_0^L \tau_0 s^* w''\, dx = \bar{F}_L + \tau_0 s^* w'(L) \tag{59}$$

Substitution of the first two boundary conditions of Table 4 and Eqs. (58) and (89) in the general solution yields the following solution for a cantilever beam based on the He and Lilley (2008) model:

$$w(x) = \frac{\bar{F}_L \cosh(L\sqrt{\varepsilon})}{K_b^{**} \varepsilon}\left[x - \frac{\tanh(L\sqrt{\varepsilon})}{\sqrt{\varepsilon}} - \frac{\sinh(x\sqrt{\varepsilon} - L\sqrt{\varepsilon})}{\sqrt{\varepsilon}\cosh(L\sqrt{\varepsilon})} \right] \tag{60}$$

Obviously, the solutions given by Eqs. (56) and (60) are different. To identify the reason for this difference we examine the boundary conditions of the He and Lilley model shown in Table 4. Note that in writing right hand side of Eqs. (58) and (59), He and Lilley (2008) assumed that a distributed load of magnitude $2b\tau_0 w''$ is acting on the beam by interpreting the right hand side of Eq. (51) as an equivalent distributed load. Furthermore, they used the expressions for stress resultants of a classical beam in the left hand side of Eqs. (58) and (59) in applying the boundary conditions. As shown here the stress resultants and natural boundary conditions for a Gurtin-Murdoch beam governed by Eq. (27) are given by Eqs. (28) and (29). Therefore, the expressions for a classical beam stress resultants used by He and Lilley to derive their solutions are not valid for a Gurtin-Murdoch beam although the governing equations of both schemes are similar [Eq. (27) and Eq. (51) respectively]. It is also noted that even though one could interpret the right hand side of Eq. (51) as equivalent to a load, it is not a physical load. This term fundamentally alters the beam governing equation as it is a function of the beam curvature and results in substantially different stress resultants and natural boundary conditions.

Based on Eq. (60), He and Lilley (2008) concluded that the cantilever nanobeam exhibits a softer elastic behaviour for $\tau_0 > 0$. They explained that the stiffer or softer behaviour of nanoscale beams is attributed to the signs of the curvature and surface stress during the static bending. The downward curvature for the cantilever nanobeams results in a positive curvature and, according to Eq. (51), a positive curvature results in a positive distributed transverse force in the same direction with the external load if $\tau_0 > 0$. Thus, the distributed transverse force increases the transverse displacement of the beam bending and the cantilever nanobeams behaves like a softer material.

The explanation of softer and stiffener behaviour of nanoscale beams using the equivalent transverse distributed force (Eq. (51)) and the signs of the curvature is questionable. Consider the governing equation of nanobeam in Eq. (27), it could be seen that the differentiation of nanobeam bending from the classical beam bending is due to the modified bending stiffness $EI - 2\nu I\tau_0 / H + (2\mu_0 + \lambda_0)I^*$ and the presence of the second order derivative term $-\tau_0 s^* d^2 w / dx^2$. Similar to the case of column buckling, the second order derivative term alter the structure of the nanobeam governing equation considerably and is primarily responsible for the diversity of

nanoscale beam behaviour from the classical beam. The interpretation of second order derivative term as a distributed force along the nanoscale beam is questionable.

We also note that the *general solutions* for beam deflection are identical for He and Lilly (2008) and Liu and Rajapakse (2010). Therefore, it can be concluded that as long as the boundary conditions are expressed in terms of deflections, slopes, bending moment and/or shear force at a cross section with zero slope, the solutions obtained from He and Lilley (2008) and Liu and Rajapakse (2010) are identical. We prove this by considering the case of simply-supported and fixed-fixed beams in the next sections.

5.2.2.2 Simply-supported beam

Table 5 summarizes the boundary conditions for a simply supported beam employed by He and Lilley (2008) and Liu and Rajapakse (2010). As the beam structure is symmetric with respect to the loading plane, the half beam model $(0 \le x \le L/2)$ can be used in the analysis.

Table 5 Comparison of boundary conditions for simply supported beams.

Liu and Rajapakse (2010)	He and Lilley (2008)
1) $w(0) = 0$	1) $w(0) = 0$
2) $M^*(0) = 0$	2) $w''(0) = 0$
3) $w'(L/2) = 0$	3) $w'(L/2) = 0$
4) $Q^*(L/2) = \dfrac{\bar{F}_L}{2}$	4) Force equilibrium at $x = 0$

In view of Eq. (28), the second boundary condition of Liu and Rajapakse [$M^*(0) = 0$] leads to $w''(0) = 0$. Therefore the first three boundary conditions of He and Lilley (2008) given in Table 5 is identical to Liu and Rajapakse (2010). Next, the substitution of the forth boundary condition of Liu and Rajapakse ($Q^*(L/2) = \bar{F}_L/2$) together with $w'(L/2) = 0$ in Eq. (28) yields,

$$-K_b^* w'''(L/2) = \frac{\bar{F}_L}{2} \tag{61}$$

Based on Eq. (54), the forth boundary condition in Table 5 given by He and Lilley (2008), i.e., force equilibrium at $x = 0$, can be written as,

$$-K_b^{**} w'''(0) + \tau_0 s^* w'(0) = \frac{\bar{F}_L}{2} \tag{62}$$

The forth boundary condition was considered by He and Lilley (2008) as

$$-K_b^{**} w'''(0) = \frac{\bar{F}_L}{2} + \int_0^{L/2} \tau_0 s^* w'' \, dx = \frac{\bar{F}_L}{2} - \tau_0 s^* w'(0) \tag{63}$$

It can be seen that Eq. (63) is identical to Eq. (62). It is also found that the solutions for simply-supported beams from the two approaches are identical. The solution for deflection of a simply-supported beam is given by

$$w(x) = \frac{\bar{F}_L}{2K_b^* \varepsilon} \left[x - \frac{\sinh(x\sqrt{\varepsilon})}{\sqrt{\varepsilon}\cosh(L\sqrt{\varepsilon}/2)} \right] \tag{64}$$

5.2.2.3 Clamped-clamped beam

Table 6 summarizes the boundary conditions for a clamped-clamped beam used by He and Lilley (2008) and Liu and Rajapakse (2010). The half beam model $(0 \le x \le L/2)$ is used in the analysis due to symmetry of the beam structure with respect to the loading plane.

Table 6 Comparison of boundary conditions for clamped-clamped beams.

Liu and Rajapakse (2010)	He and Lilley (2008)
1) $w(0) = 0$	1) $w(0) = 0$
2) $w'(0) = 0$	2) $w'(0) = 0$
3) $w'(L/2) = 0$	3) $w'(L/2) = 0$
4) $Q^*(L/2) = \frac{\bar{F}_L}{2}$	4) Force equilibrium at $x = 0$

The first three boundary conditions are identical. The forth boundary conditions for Liu and Rajapakse (2010) and He and Lilley (2008) beam models are given in Eqs. (61) and (63) respectively. It can be shown that the two models again result in identical solutions for clamped-clamped beams. The solution for deflection of a clamped-clamped beam is obtained as

$$w(x) = \frac{\bar{F}_L}{2K_b^* \varepsilon} \left[x - \frac{\sinh(x\sqrt{\varepsilon} - L\sqrt{\varepsilon}/4) + \sinh(L\sqrt{\varepsilon}/4)}{\sqrt{\varepsilon}\cosh(L\sqrt{\varepsilon}/4)} \right] \tag{65}$$

6. Conclusion

Mechanistic models incorporating surface stress effects based on the Gurtin-Murdoch surface elasticity theory are developed to analyze nanoscale beams and rectangular plates. Closed-form analytical solutions for rectangular nanoplates can be derived for certain plate configurations. A finite element formulation for nanoplates is successfully developed based on the weighted residual method. Numerical results indicate that the static and dynamic responses are significantly influenced by surface energy effects and plate boundary conditions. Highest influence of the surface energy effect is observed for simply-supported plates followed by SCSC plates and only minor effects are noted for clamped plates. This behavior is consistent with the fact that the surface stress contribution associated with Young-Laplace effect is controlled by the curvature of plate. Plates with smaller radius of curvature (simply-supported) therefore show the highest effect of surface stress. First natural frequency of plates shows a substantial effect of surface stress but the influence diminishes for higher natural frequencies. However, mode shapes show negligible influence of surface energy effects.

A variational approach was used to re-derive the governing equation and admissible boundary conditions for a beam based on Gurtin-Murdoch surface elasticity theory. The new governing equation is identical to that derived by Liu and Rajapakse (2010) by considering equilibrium of an infinitesimal beam element. The governing equation derived by He and Lilley (2008) has the same structure, but the modified stiffnesses are different from Liu and Rajapakse (2010) and the present study. The admissible boundary condtions are also obtained from the variational formulation, which is identical to the resultant shear and moment at section given by Liu and Rajapakse (2010). On the other hand, the shear force and moment condition used by He and Lilley (2010) were based on the classical beam theory does not agree with the natural boundary condition from the variational formulation. He and Lilley solutions for nanobeams were determined by using essential boundary conditions and these force and/or moment equilibrium conditions at the origin. However, the condition of equilibrium at the beam origin, depending on the beam type, may fail meet the requirement at the other beam end and as a result cantilever beams shows behaviour different from other beams.

7. Output

7.1 International Journal Publication and Manuscript

1. Y. Sapsathiarn and R.K.N.D. Rajapakse (2016) Static and Dynamic Analyses of Nanoscale Rectangular Plates Incorporating Surface Energy. *Acta Mechanica*, DOI 10.1007/s00707-015-1521-1, pp. 1-15. [Received: 31 March 2015 / Revised: 6 July 2015 / Published Online: 11 January 2016]

2. The manuscript “Mechanistic Models and Variational Formulation of Nano-scale Beam Bending” by Y. Sapsathiarn and R.K.N.D. Rajapakse is to be submitted to Nano Letters in August 2016.

7.2 Others

1. Y. Sapsathiarn and R.K.N.D. Rajapakse (2014) Static and dynamic analysis of nanoscale rectangular plates incorporating surface energy. The Fourth Asian Conference on Mechanics of Functional Materials and Structures (ACMFMS2014). 2014: 907406 [*Invited*].

References:

Chen, T.Y., Chiu, M.S. and Weng, C.N.: Derivation of the generalized Young–Laplace equation of curved interfaces in nanoscaled solids. J. Appl. Phys., 100, 074308, (2006).

Gere, J.M. and Timoshenko, S.P.: Mechanics of materials, Chapman & Hall, London, England (1991).

Gurtin, M.E. and Murdoch, A.I.: A Continuum Theory of Elastic Material Surfaces. Archive for Rational Mechanics and Analysis 57, 291–323 (1975).

Gurtin, M.E. and Murdoch, A.I.: Addenda to our paper: A continuum theory of elastic material surfaces. Archive for Rational Mechanics and Analysis 59, 389–390 (1975).

Laplace, P.S. Traité de mécanique céleste, Gauthier-Villars, Paris, Vol. 4, Supplements au Livre X, 771-777 (1805).

Liu C. and Rajapakse R.K.N.D.: Continuum models incorporating surface energy for static and dynamic response of nanoscale beams. IEEE Transaction on Nanotechnology 9, 422–431 (2010).

Lu, P. He, L.H. Lee, H.P. and Lu, C.: Thin plate theory including surface effects. Int. J. Solids Struct., 43, 4631–4647 (2006).

Miller, R.E. and Shenoy, V.B.: Size-dependent elastic properties of nanosized structural elements. Nanotechnology 11, 139–147 (2000).

Sapsathiarn, Y. and Rajapakse, R.K.N.D.: Static and dynamic analyses of nanoscale rectangular plates incorporating surface energy. Acta Mechanica, 1-15 (2016).

Shenoy, V.B.: Atomistic calculations of elastic properties of metallic fcc crystal surfaces. Physical Review B 71, 094104-1–094104-11 (2005).

Timoshenko, S.P. and Woinowsky-Krieger, S.: Theory of plates and shells, McGraw Hill, New York (1959).

Washizu, K.: Variational methods in elasticity and plasticity, 2nd Ed., New York, Pergamon (1982).

Young, T.: An Essay on the Cohesion of Fluids. Philos. Trans. R. Soc. London,95, 65-87 (1805).

Zienkiewicz, O.C., and Taylor, R.L.: The Finite Element Method, Fifth Ed., Butterworth-Heinemann, Boston (2000).

Acta Mech
DOI 10.1007/s00707-015-1521-1

ORIGINAL PAPER

Y. Sapsathiarn · R. K. N. D. Rajapakse

Static and dynamic analyses of nanoscale rectangular plates incorporating surface energy

Received: 31 March 2015 / Revised: 6 July 2015

Abstract In this paper, the Gurtin–Murdoch continuum theory is applied to develop a new continuum mechanics model for static and dynamic analyses of nanoscale rectangular plates. The relevant governing equations are established from basic principles. Analytical solutions for static and free vibration of nanoscale rectangular plates are presented for selected boundary conditions. A finite element method for the analysis of rectangular nanoplates is also developed to solve general cases that cannot be solved analytically. Expressions for stiffness and mass matrices and the load vector are derived by using a weighted residual formulation. A selected set of numerical results is presented to investigate the size-dependent static and free vibration response of plates and the influence of surface material properties and boundary conditions.

1 Introduction

Nanoplates are key elements of various nanotechnology-based devices such as nanoelectromechanical systems (NEMS), sensors [1]. Successful design and manufacture of nanoscale devices require thorough understanding of their mechanical properties and deformations.

Various modeling approaches have been proposed to investigate the behavior of nanostructures. Atomistic simulations [2] provide a strong theoretical basis to analyze nanostructures, but such simulations are computationally prohibitive when applied at a device/system level. Modified continuum mechanics models based on a theory proposed by Gurtin and Murdoch [3,4] that incorporates the effects of surface energy have been widely used in the literature for the analysis of nanostructures due to their computational efficiency and versatility [3–10]. A nanoplate model based on the Gurtin–Murdoch continuum theory is considered to have a bulk material region and an elastic surface with mathematically zero thickness. The surface elastic constants are different from those of the bulk and can be determined by atomistic computations [2,11,12].

In this paper, a mechanistic model incorporating the effects of surface energy based on the Gurtin–Murdoch surface elasticity theory [3,4] is developed to analyze the response of rectangular nanoplates. Rectangular geometry is commonly encountered in the development of NEMS-based devices. Previous studies have developed models for circular nanoplates, nanofilms and nanobeams [5–10]. A set of closed-form analytical solutions and a finite element formulation for static and dynamic analyses of nanoplates are presented. Selected numerical results are presented to portray the size-dependent response of nanoplates and the influence of surface properties and boundary conditions.

Y. Sapsathiarn (✉)
Department of Civil and Environmental Engineering, Faculty of Engineering, Mahidol University,
Nakhon Pathom 73170, Thailand
E-mail: yasothorn.sap@mahidol.ac.th

R. K. N. D. Rajapakse
Carleton University, Ottawa K1S 5B6, Canada

Published online: 11 January 2016

2 Formulation of governing equations

Consider an incremental element of a thin rectangular nanoplate with a Cartesian coordinate system (x, y, z) as shown in Fig. 1. It is assumed that the response of the plate is governed by the continuum theory proposed by Gurtin and Murdoch [3,4], and its deflections are small and strains are infinitesimal. According to the Gurtin–Murdoch theory [3,4], the plate element consists of a bulk material and surface layer of zero mathematical thickness. Stresses acting on the surface and bulk incremental elements are shown in Fig. 1a, b, respectively. The elastic properties of a surface element are surface Lamé constants λ_0 and μ_0, surface residual stress under unstrained conditions τ_0, and the surface mass density (defined as the mass of atoms of a unit surface area) ρ_0. From Gurtin–Murdoch theory [3,4],

$$\tau^{\pm}_{\alpha\beta} = \tau_0\delta_{\alpha\beta} + (\mu_0 - \tau_0)\left(u^{\pm}_{\alpha,\beta} + u^{\pm}_{\beta,\alpha}\right) + (\tau_0 + \lambda_0)u^{\pm}_{\gamma,\gamma}\delta_{\alpha\beta} + \tau_0 u^{\pm}_{\alpha,\beta}, \tag{1.1}$$

$$\tau^{\pm}_{\alpha z} = \tau_0 u^{\pm}_{z,\alpha} \tag{1.2}$$

where $\tau^{\pm}_{\alpha\beta}(\alpha, \beta = x, y)$ with superscripts '+' and '−' denoting the surface stress components of the top and bottom surfaces, respectively.

The force equilibrium equations of the top (Fig. 1a) and bottom surfaces can be expressed as

$$\tau^{+}_{\alpha i,\alpha} - \sigma^{+}_{zi} = \rho^{+}_0 \ddot{u}^{+}_i, \tag{2.1}$$

$$\tau^{-}_{\alpha i,\alpha} + \sigma^{-}_{zi} = \rho^{-}_0 \ddot{u}^{-}_i \tag{2.2}$$

where $\sigma^{+}_{zi}(i = x, y, z)$ are the resulting contact tractions existing on the interface of bulk and top surface layers due to the interaction between the surface layer and bulk.

Equilibrium of an incremental element of the bulk (Fig. 1b) in the x-direction can be expressed as:

$$\int_{-h/2}^{h/2} \frac{\partial \sigma_{xx}}{\partial x}\mathrm{d}z + \int_{-h/2}^{h/2} \frac{\partial \sigma_{yx}}{\partial y}\mathrm{d}z + \sigma^{+}_{zx} - \sigma^{-}_{zx} + \int_{-h/2}^{h/2} b_x \mathrm{d}z = \int_{-h/2}^{h/2} \rho \ddot{u}_x \mathrm{d}z \tag{3}$$

where σ_{ij}, b_i and ρ are bulk stresses, body forces and mass density of the bulk material, respectively; and h is the thickness of the plate.

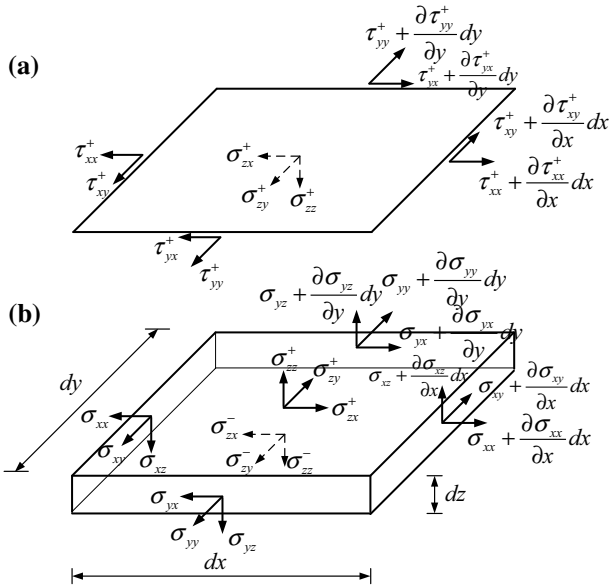

Fig. 1 **a** Surface stresses on an incremental element of the top surface layer; and **b** stress components of an incremental bulk element

Similarly, the equilibrium of the bulk element in the y- and z-directions, respectively, yields,

$$\int_{-h/2}^{h/2} \frac{\partial \sigma_{xy}}{\partial x} \mathrm{d}z + \int_{-h/2}^{h/2} \frac{\partial \sigma_{yy}}{\partial y} \mathrm{d}z + \sigma_{zy}^{+} - \sigma_{zy}^{-} + \int_{-h/2}^{h/2} b_y \mathrm{d}z = \int_{-h/2}^{h/2} \rho \ddot{u}_y \mathrm{d}z, \tag{4.1}$$

$$\int_{-h/2}^{h/2} \frac{\partial \sigma_{xz}}{\partial x} \mathrm{d}z + \int_{-h/2}^{h/2} \frac{\partial \sigma_{yz}}{\partial y} \mathrm{d}z + \sigma_{zz}^{+} - \sigma_{zz}^{-} + \int_{-h/2}^{h/2} b_z \mathrm{d}z + q(x, y) = \int_{-h/2}^{h/2} \rho \ddot{u}_z \mathrm{d}z \tag{4.2}$$

where $q(x, y)$ denotes the applied loading on the plate.

Next, the moment equilibrium equations of the bulk element about the y-axis and x-axis can be expressed as:

$$\int_{-h/2}^{h/2} \left(\frac{\partial \sigma_{xx}}{\partial x} + \frac{\partial \sigma_{yx}}{\partial y} \right) z \mathrm{d}z + \frac{h}{2} \left(\sigma_{zx}^{+} + \sigma_{zx}^{-} \right) - \int_{-h/2}^{h/2} \sigma_{xz} \mathrm{d}z + \int_{-h/2}^{h/2} b_x z \mathrm{d}z = \int_{-h/2}^{h/2} \rho \ddot{u}_x z \mathrm{d}z, \tag{5.1}$$

and $$\int_{-h/2}^{h/2} \left(\frac{\partial \sigma_{xy}}{\partial x} + \frac{\partial \sigma_{yy}}{\partial y} \right) z \mathrm{d}z + \frac{h}{2} \left(\sigma_{zy}^{+} + \sigma_{zy}^{-} \right) - \int_{-h/2}^{h/2} \sigma_{yz} \mathrm{d}z + \int_{-h/2}^{h/2} b_y z \mathrm{d}z = \int_{-h/2}^{h/2} \rho \ddot{u}_y z \mathrm{d}z. \tag{5.2}$$

Assume that the bulk material is homogeneous and isotropic and let E and ν denote its Young's modulus and Poisson's ratio, respectively. Its constitutive relations can be expressed as

$$\sigma_{xx} = \frac{E}{1-\nu^2} \varepsilon_{xx} + \frac{E\nu}{1-\nu^2} \varepsilon_{yy} + \frac{\nu}{1-\nu} \sigma_{zz}, \tag{6.1}$$

$$\sigma_{yy} = \frac{E}{1-\nu^2} \varepsilon_{yy} + \frac{E\nu}{1-\nu^2} \varepsilon_{xx} + \frac{\nu}{1-\nu} \sigma_{zz}, \tag{6.2}$$

$$\sigma_{i\alpha} = \frac{E}{1-\nu^2} \varepsilon_{i\alpha}. \tag{6.3}$$

In the present paper, the bulk stress σ_{zz} is assumed to vary linearly through the plate thickness to satisfy the equilibrium conditions on the surface. Therefore,

$$\sigma_{zz} = \frac{1}{2} \left(\sigma_{zz}^{+} + \sigma_{zz}^{-} \right) + \frac{z}{h} \left(\sigma_{zz}^{+} - \sigma_{zz}^{-} \right). \tag{7}$$

Rewriting σ_{zz} in terms of surface stresses using Eq. (2) and assuming $\rho_0^{+} = \rho_0^{-} = \rho_0$ yields

$$\sigma_{zz} = \frac{1}{2} \left(\tau_{\alpha z,\alpha}^{+} - \tau_{\alpha z,\alpha}^{-} - \rho_0 \ddot{u}_z^{+} + \rho_0 \ddot{u}_z^{-} \right) + \frac{z}{h} \left(\tau_{\alpha z,\alpha}^{+} + \tau_{\alpha z,\alpha}^{-} - \rho_0 \ddot{u}_z^{+} - \rho_0 \ddot{u}_z^{-} \right). \tag{8}$$

For a Kirchhoff plate,

$$u_x = -z \frac{\partial w}{\partial x}; \quad u_y = -z \frac{\partial w}{\partial y}; \quad u_z = w(x, y) \tag{9}$$

where $w(x, y)$ denotes the vertical displacement of the plate.

The relevant strain–displacement relations for the bulk materials are

$$\varepsilon_{xx} = -z \frac{\partial^2 w}{\partial x^2}; \quad \varepsilon_{yy} = -z \frac{\partial^2 w}{\partial y^2}; \quad \varepsilon_{xy} = -z \frac{\partial^2 w}{\partial x \partial y}, \tag{10}$$

and $\varepsilon_{xz} = \varepsilon_{yz} = \varepsilon_{zz} = 0$.

After further manipulations, the following governing equation for a thin plate incorporating the effects of surface energy can be obtained based on Eqs. (1)–(10):

$$D^*\left(\frac{\partial^4 w}{\partial x^4}+2\frac{\partial^4 w}{\partial x^2\partial y^2}+\frac{\partial^4 w}{\partial y^4}\right)-2\tau_0\left(\frac{\partial^2 w}{\partial x^2}+\frac{\partial^2 w}{\partial y^2}\right)+q(x,y)$$
$$=-(\rho h+2\rho_0)\frac{\partial^2 w}{\partial t^2}+\left(\frac{\rho^3 h}{12}+\frac{\rho_0 h^2}{2}-\frac{\rho_0 h^2\nu}{6(1-\nu)}\right)\left(\frac{\partial^4 w}{\partial x^2\partial t^2}+\frac{\partial^4 w}{\partial y^2\partial t^2}\right) \tag{11}$$

where $D^*=\frac{Eh^3}{12(1-\nu^2)}+\frac{h^2}{2}(2\mu_0+\lambda_0)-\frac{h^2\tau_0\nu}{6(1-\nu)}$.

3 Analytical solutions

3.1 Static loading

For static problems, the governing equation, Eq. (11), is simplified to

$$D^*\nabla^2\nabla^2 w-2\tau_0\nabla^2 w+q(x,y)=0,\quad 0<x<a,\quad 0<y<b \tag{12}$$

where $\nabla^2=\frac{\partial^2}{\partial x^2}+\frac{\partial^2}{\partial y^2}$.

3.1.1 Plates with all edges simply supported (SSSS)

Consider a rectangular plate of dimensions a and b in the x- and y-directions with all edges simply supported and subject to a distributed loading of the form:

$$q(x,y)=\sum_{m=1}^{\infty}\sum_{n=1}^{\infty}q_{mn}\sin\frac{m\pi x}{a}\sin\frac{n\pi y}{b},\quad 0<x<a,\quad 0<y<b. \tag{13}$$

Boundary conditions are:

$$w=0|_{x=0,a};\quad w=0|_{y=0,b}, \tag{14.1}$$
$$M_x^*=0|_{x=0,a};\quad M_y^*=0|_{y=0,b} \tag{14.2}$$

where

$$M_x^*=-D^*\frac{\partial^2 w}{\partial x^2}-D_1\frac{\partial^2 w}{\partial y^2};\quad M_y^*=-D^*\frac{\partial^2 w}{\partial y^2}-D_1\frac{\partial^2 w}{\partial x^2} \tag{15}$$

and $D_1=\frac{Eh^3\nu}{12(1-\nu^2)}+\frac{h^2}{2}(\lambda_0+\tau_0)$.

Observing that, since $w=0$ at all edges (from boundary conditions), therefore, $\partial^2 w/\partial x^2=0$ for the edges parallel to the x-axis and $\partial^2 w/\partial y^2=0$ for the edges parallel to the y-axis. Using expression (15) for M_x^* and M_y^*, boundary conditions (14.2) can be written as

$$\left.\frac{\partial^2 w}{\partial x^2}=0\right|_{x=0,a};\qquad \left.\frac{\partial^2 w}{\partial y^2}=0\right|_{y=0,b}. \tag{16}$$

The deflection function of a simply supported plate can be represented by a double Fourier series of the form:

$$w(x,y)=\sum_{m=1}^{\infty}\sum_{n=1}^{\infty}w_{mn}\sin\frac{m\pi x}{a}\sin\frac{n\pi y}{b}. \tag{17}$$

Substituting Eqs. (13) and (17) into Eq. (12) and equating coefficients, the unknown coefficients in Eq. (17) can be obtained as

$$w_{mn}=\frac{-q_{mn}}{D^*\pi^4\left(\frac{m^2}{a^2}+\frac{n^2}{b^2}\right)^2+2\tau_0\pi^2\left(\frac{m^2}{a^2}+\frac{n^2}{b^2}\right)}. \tag{18}$$

For a uniformly distributed load, $q(x, y) = q_0$:

$$q_{mn} = \frac{4q_0}{\pi^2 mn}(1 - \cos m\pi)(1 - \cos n\pi). \tag{19.1}$$

For a concentrated load P_0 at the point (a', b'):

$$q_{mn} = \frac{4P_0}{ab} \sin \frac{m\pi a'}{a} \sin \frac{n\pi b'}{b}. \tag{19.2}$$

The plate stress resultants can be determined by using Eq. (15) and Eqs. (17)–(19).

SSSS plates on elastic substrate

Nanoplates that are placed on an elastic substrate can be modeled as a plate on a Winkler foundation. For plates on an elastic substrate with Winkler constant k, the governing equation is

$$D^*\nabla^2\nabla^2 w - 2\tau_0\nabla^2 w - kw + q(x) = 0. \tag{20}$$

The solution for plates with simply supported edges resting on elastic substrate is given by Eq. (17) with

$$w_{mn} = \frac{-q_{mn}}{D^*\pi^4\left(\frac{m^2}{a^2} + \frac{n^2}{b^2}\right)^2 + 2\tau_0\pi^2\left(\frac{m^2}{a^2} + \frac{n^2}{b^2}\right) - k}. \tag{21}$$

3.1.2 Plates with two opposite edges simply supported and remaining edges clamped (SCSC)

To derive the solution of an SCSC plate, consider first a plate with two opposite edges $x = 0$ and $x = a$ simply supported. When the load distribution q is a function of x only and represented in the form $q = \sum_{m=1}^{\infty} q_m \sin \frac{m\pi x}{a}$ where q_m is a constant, the deflection of the plate can be expressed in the form of [13],

$$w(x, y) = w_1 + \sum_{m=1}^{\infty} Y_m \sin \frac{m\pi x}{a}, \quad 0 < x < a, \quad -\frac{b}{2} < y < \frac{b}{2}, \tag{22}$$

in which w_1 satisfies the boundary conditions at $x = 0$ and $x = a$; and Y_m is a function of y only and satisfies the boundary condition at $y = \pm b/2$.

Boundary conditions for a SCSC plate are given by

$$w = 0|_{x=0,a}; \quad \left.\frac{d^2 w}{dx^2} = 0\right|_{x=0,a}; \tag{23.1}$$

$$w = 0|_{y=\pm\frac{b}{2}}; \quad \left.\frac{dw}{dy} = 0\right|_{y=\pm\frac{b}{2}}, \tag{23.2}$$

The function w_1 can be determined from

$$D^*\frac{d^4 w_1}{dx^4} - 2\tau_0\frac{d^4 w_1}{dx^4} + q(x) = 0 \tag{24}$$

subjected to the boundary conditions

$$w_1 = 0|_{x=0,a}; \quad \left.\frac{d^2 w_1}{dx^2} = 0\right|_{x=0,a}. \tag{25}$$

It can be shown that the solution w_1 for loading $q = \sum_{m=1}^{\infty} q_m \sin \frac{m\pi x}{a}$ can be obtained as

$$w_1 = -\sum_{m=1}^{\infty} \frac{q_m}{D^*\pi^4\frac{m^4}{a^4} + 2\tau_0\pi^2\frac{m^2}{a^2}} \sin \frac{m\pi x}{a}. \tag{26}$$

The function Y_m must satisfy the homogeneous differential equation

$$D^*\nabla^2\nabla^2\left(\sum_{m=1}^{\infty} Y_m \sin\frac{m\pi x}{a}\right) - 2\tau_0\nabla^2\left(\sum_{m=1}^{\infty} Y_m \sin\frac{m\pi x}{a}\right) = 0. \tag{27}$$

It can be proved that the general solution of Y_m can be expressed as

$$Y_m = A_m e^{\frac{m\pi y}{a}} + B_m e^{-\frac{m\pi y}{a}} + C_m e^{y\sqrt{(\frac{m\pi}{a})^2+\frac{2\tau_0}{D^*}}} + D_m e^{-y\sqrt{(\frac{m\pi}{a})^2+\frac{2\tau_0}{D^*}}} \tag{28}$$

where the four constants A_m, B_m, C_m, D_m are to be determined from the plate boundary conditions along $y = \pm b/2$.

From Eqs. (22), (27) and (28), the deflection of the SCSC plate can be written as

$$w(x,y) = \sum_{m=1}^{\infty}\left[A_m e^{\frac{m\pi y}{a}} + B_m e^{-\frac{m\pi y}{a}} + C_m e^{y\sqrt{(\frac{m\pi}{a})^2+\frac{2\tau_0}{D^*}}} + D_m e^{-y\sqrt{(\frac{m\pi}{a})^2+\frac{2\tau_0}{D^*}}}\right]\sin\frac{m\pi x}{a}$$
$$-\sum_{m=1}^{\infty}\frac{q_m}{D^*\pi^4\frac{m^4}{a^4}+2\tau_0\pi^2\frac{m^2}{a^2}}\sin\frac{m\pi x}{a}. \tag{29}$$

It can be proved that the boundary condition in (23.1) is automatically satisfied by the solution in Eq. (29). Substitution of Eq. (29) into the boundary condition in (23.2) yields a set of equations for determining the coefficients A_m, B_m, C_m, D_m, and the following solutions for these coefficients are obtained:

$$A_m = B_m = -\frac{q_m\sqrt{(\frac{m\pi}{a})^2-\frac{2\tau_0}{D^*}}\left(e^{b\sqrt{(\frac{m\pi}{a})^2+\frac{2\tau_0}{D^*}}}-1\right)\left(e^{\frac{m\pi b}{2a}}\right)}{\Omega\left(D^*\pi^4\frac{m^4}{a^4}+2\tau_0\pi^2\frac{m^2}{a^2}\right)}, \tag{30.1}$$

$$C_m = D_m = \frac{q_m\left(\frac{m\pi}{a}\right)\left(e^{\frac{m\pi b}{a}}-1\right)\left(e^{\frac{b}{2}\sqrt{(\frac{m\pi}{a})^2+\frac{2\tau_0}{D^*}}}\right)}{\Omega\left(D^*\pi^4\frac{m^4}{a^4}+2\tau_0\pi^2\frac{m^2}{a^2}\right)} \tag{30.2}$$

where $\Omega = \left(\frac{m\pi}{a}\right)\left(e^{\frac{m\pi b}{a}}-1\right)\left(e^{b\sqrt{(\frac{m\pi}{a})^2+\frac{2\tau_0}{D^*}}}+1\right) - \sqrt{(\frac{m\pi}{a})^2-\frac{2\tau_0}{D^*}}\left(e^{\frac{m\pi b}{a}}+1\right)\left(e^{b\sqrt{(\frac{m\pi}{a})^2+\frac{2\tau_0}{D^*}}}-1\right)$;

$$\text{and for a uniformly distributed load } q_0: \; q_m = \frac{2q_0}{\pi m}\left\{1-(-1)^m\right\}; \tag{31.1}$$

$$\text{and for a line load } q_0 \text{ along } x = l: \; q_m = \frac{2q_0}{a}\sin\frac{m\pi l}{a}, \tag{31.2}$$

3.2 Free vibration analysis

Free vibration characteristics (natural frequencies and mode shapes) of nanoscale plates are an important consideration in the design of NEMS and other nanodevices. Based on Eq. (11), the governing equation for free vibration of a rectangular nanoscale plate is

$$D^*\left(\frac{\partial^4 w}{\partial x^4}+2\frac{\partial^4 w}{\partial x^2\partial y^2}+\frac{\partial^4 w}{\partial y^4}\right) - 2\tau_0\left(\frac{\partial^2 w}{\partial x^2}+\frac{\partial^2 w}{\partial y^2}\right) + (\rho h + 2\rho_0)\frac{\partial^2 w}{\partial t^2}$$
$$-\left(\frac{\rho^3 h}{12}+\frac{\rho_0 h^2}{2}-\frac{\rho_0 h^2\nu}{6(1-\nu)}\right)\left(\frac{\partial^4 w}{\partial x^2\partial t^2}+\frac{\partial^4 w}{\partial y^2\partial t^2}\right) = 0. \tag{32}$$

3.2.1 Plates with all edges simply supported

The dynamic response of a simply supported nanoplate undergoing time-harmonic oscillations at frequency ω can be represented as

$$w(x, y, t) = \sum_{m=1}^{\infty} \sum_{n=1}^{\infty} w_{mn} \sin \frac{m\pi x}{a} \sin \frac{n\pi y}{b} e^{i\omega t}, \quad 0 < x < a, \quad .0 < y < b. \tag{33}$$

Substitution of w from Eq. (33) into Eq. (32) yields the following solution for the natural frequencies of the plate:

$$\omega_{mn}^2 = \frac{D^* \left(\lambda_m^2 + \lambda_n^2\right)^2 + 2\tau_0 \left(\lambda_m^2 + \lambda_n^2\right)}{(\rho h + 2\rho_0) + \left(\frac{\rho^3 h}{12} + \frac{\rho_0 h^2}{2} - \frac{\rho_0 h^2 \nu}{6(1-\nu)}\right)\left(\lambda_m^2 + \lambda_n^2\right)}, \quad m, n = 1, 2, 3, \ldots \tag{34}$$

where $\lambda_m = m\pi/a$ and $\lambda_n = n\pi/b$.

3.2.2 SCSC plates

Assuming that the edges $x = 0$ and $x = a$ are simply supported, the dynamic response of the plate can be expressed as

$$w = \sum_{m=1}^{\infty} Y_m \sin \frac{m\pi x}{a} e^{i\omega t}, \quad 0 < x < a, \quad -\frac{b}{2} < y < \frac{b}{2}. \tag{35}$$

Substituting Eq. (35) into Eq. (32) and consideration of each harmonic m yield

$$\begin{aligned} &D^* \left[\left(\frac{m\pi}{a}\right)^4 Y_m - 2\left(\frac{m\pi}{a}\right)^2 \frac{d^2 Y_m}{dy^2} + \frac{d^4 Y_m}{dy^4} \right] - 2\tau_0 \left[-\left(\frac{m\pi}{a}\right)^2 Y_m + \frac{d^2 Y_m}{dy^2} \right] \\ &-(\rho h + 2\rho_0)\omega^2 Y_m + \left(\frac{\rho^3 h}{12} + \frac{\rho_0 h^2}{2} - \frac{\rho_0 \tau_0 h^2 \nu}{6(1-\nu)}\right) \omega^2 \left[-\left(\frac{m\pi}{a}\right)^2 Y_m + \frac{d^2 Y_m}{dy^2} \right] = 0. \end{aligned} \tag{36}$$

The solution of Y_m in Eq. (36) can be expressed as

$$Y_m = A_m e^{y\sqrt{\lambda_m^2 + \gamma - \beta}} + B_m e^{-y\sqrt{\lambda_m^2 + \gamma - \beta}} + C_m e^{y\sqrt{\lambda_m^2 + \gamma + \beta}} + D_m e^{-y\sqrt{\lambda_m^2 + \gamma + \beta}} \tag{37}$$

where $\lambda_m = \frac{m\pi}{a}$; $\gamma = \tau_0 - \left(\frac{\rho^3 h}{6} + \rho_0 h^2 - \frac{\rho_0 h^2 \nu}{3(1-\nu)}\right)\omega^2$ and $\beta = \sqrt{(\rho h + 2\rho_0)\omega^2 + \gamma^2}$.

The four constants A_m, B_m, C_m, D_m in Eq. (37) are to be determined from plate boundary conditions along the $y = \pm b/2$ edges. The substitution of Y_m in Eq. (37) into the boundary conditions at $y = \pm b/2$ [see Eq. (23.2)] yields the frequency equation from which ω can be determined using numerical techniques.

4 Finite element formulation

4.1 Formulation for static loading

Galerkin's weighted residual method is now applied to Eq. (12) to develop the finite element (FE) formulation for plates. Following Zienkiewicz and Taylor [14], the weighted residual statement for static loading is:

$$\int_V \bar{w} \left\{ D^* \left(\frac{\partial^4 w}{\partial x^4} + 2\frac{\partial^4 w}{\partial x^2 \partial y^2} + \frac{\partial^4 w}{\partial y^4} \right) - 2\tau_0 \left(\frac{\partial^2 w}{\partial x^2} + \frac{\partial^2 w}{\partial y^2} \right) + q(x, y) \right\} \mathrm{d}V = 0 \tag{38}$$

where V denotes the volume of the plate and $\bar{w}$ is the weight function.

Integrating Eq. (38) by parts, the weak formulation can be written as

$$\int\int_{\Omega_0} \left\{ D^* \frac{\partial^2 \bar{w}}{\partial x^2} \left(\frac{\partial^2 w}{\partial x^2} + \nu \frac{\partial^2 w}{\partial y^2} \right) + D^* \frac{\partial^2 \bar{w}}{\partial y^2} \left(\frac{\partial^2 w}{\partial y^2} + \nu \frac{\partial^2 w}{\partial x^2} \right) + 2(1-\nu) D^* \left(\frac{\partial^2 \bar{w}}{\partial x \partial y} \frac{\partial^2 w}{\partial x \partial y} \right) + 2\tau_0 \left(\frac{\partial \bar{w}}{\partial x} \frac{\partial w}{\partial x} + \frac{\partial \bar{w}}{\partial y} \frac{\partial w}{\partial y} \right) + \bar{w} q \right\} \mathrm{d}x\mathrm{d}y = 0. \tag{39}$$

A 4-node rectangular finite element with $w, \theta_x [=\partial w/\partial x]$ and $\theta_y [=\partial w/\partial y]$ as the nodal variables is considered. The element nodal displacement vector can be written as

$$\{w^e\} = \left[w^1 \theta_x^1 \theta_y^1 \ldots w^4 \theta_x^4 \theta_y^4 \right]^{\mathrm{T}}. \tag{40}$$

Vertical displacement, w, is interpolated by using a set of shape functions as

$$w = \mathbf{N}\mathbf{w}^e = N_{11} w^1 + N_{12} \theta_x^1 + N_{13} \theta_y^1 + \cdots + N_{41} w^4 + N_{42} \theta_x^4 + N_{43} \theta_y^4 \tag{41}$$

where

$$N_{i1} = \frac{1}{8}(1+\xi_0)(1+\eta_0)\left(2+\xi_0+\eta_0-\xi^2-\eta^2\right), \tag{42.1}$$

$$N_{i2} = \frac{1}{8}\xi_i(\xi_0-1)(1+\eta_0)(1+\xi_0)^2, \tag{42.2}$$

$$N_{i3} = \frac{1}{8}\eta_i(\eta_0-1)(1+\eta_0)(1+\eta_0)^2, \tag{42.3}$$

$$\xi = \frac{x-x_0}{a}; \quad \eta = \frac{y-y_0}{b}; \quad \xi_0 = \xi\xi_i; \quad \eta_0 = \eta\eta_i \tag{42.4}$$

in which (x_0, y_0) are the global coordinates of the center of a rectangular plate finite element.

Substitution of Eq. (41) into Eq. (39) yields the element stiffness matrix ($\mathbf{K}^e$) and nodal force vector ($\mathbf{f}^e$) as

$$\mathbf{K}^e = \int_{\Omega_0} \left\{ \mathbf{B}_2^T \mathbf{C} \mathbf{B}_2 + 2\tau_0 \mathbf{B}_1^T \mathbf{B}_1 \right\} \mathrm{d}x\mathrm{d}y; \quad \mathbf{f}^e = \int_{\Omega_0} \mathbf{N} q \, \mathrm{d}x\mathrm{d}y \tag{43}$$

where

$$\mathbf{B}_1 = \begin{bmatrix} \frac{\partial N_{11}}{\partial x} & \frac{\partial N_{12}}{\partial x} & \frac{\partial N_{13}}{\partial x} & \cdots & \frac{\partial N_{41}}{\partial x} & \frac{\partial N_{42}}{\partial x} & \frac{\partial N_{43}}{\partial x} \\ \frac{\partial N_{11}}{\partial y} & \frac{\partial N_{12}}{\partial y} & \frac{\partial N_{13}}{\partial y} & \cdots & \frac{\partial N_{41}}{\partial y} & \frac{\partial N_{42}}{\partial y} & \frac{\partial N_{43}}{\partial y} \end{bmatrix}, \tag{44.1}$$

$$\mathbf{B}_2 = \begin{bmatrix} \frac{\partial^2 N_{11}}{\partial x^2} & \frac{\partial^2 N_{12}}{\partial x^2} & \frac{\partial^2 N_{13}}{\partial x^2} & \cdots & \frac{\partial^2 N_{41}}{\partial x^2} & \frac{\partial^2 N_{42}}{\partial x^2} & \frac{\partial^2 N_{43}}{\partial x^2} \\ \frac{\partial^2 N_{11}}{\partial y^2} & \frac{\partial^2 N_{12}}{\partial y^2} & \frac{\partial^2 N_{13}}{\partial y^2} & \cdots & \frac{\partial^2 N_{41}}{\partial y^2} & \frac{\partial^2 N_{42}}{\partial y^2} & \frac{\partial^2 N_{43}}{\partial y^2} \\ 2\frac{\partial^2 N_{11}}{\partial x \partial y} & 2\frac{\partial^2 N_{12}}{\partial x \partial y} & 2\frac{\partial^2 N_{13}}{\partial x \partial y} & \cdots & 2\frac{\partial^2 N_{41}}{\partial x \partial y} & 2\frac{\partial^2 N_{42}}{\partial x \partial y} & 2\frac{\partial^2 N_{43}}{\partial x \partial y} \end{bmatrix}, \tag{44.2}$$

$$\mathbf{C} = \begin{bmatrix} D^* & \nu D^* & 0 \\ \nu D^* & D^* & 0 \\ 0 & 0 & \frac{(1-\nu)D^*}{2} \end{bmatrix}. \tag{44.3}$$

It can be seen from Eq. (43) that the surface stresses contribute to the stiffness matrix of a plate element. In the absence of surface stress effects, the stiffness matrix reduces to the classical elasticity case. The assembly of element stiffness matrices and nodal force vectors yields the following global equilibrium equation:

$$\mathbf{K}\mathbf{r} = \mathbf{f} \tag{45}$$

where $\mathbf{K}$, $\mathbf{r}$ and $\mathbf{f}$ are the global stiffness matrix, global nodal force vector and global generalized displacement vector, respectively.

4.2 Free vibration problem

For a dynamic analysis, the inertia terms on the right-hand side of Eq. (11) have to be considered in the finite element formulation, and these terms correspond to the element mass matrix. It can be shown that the element mass matrix is given by

$$\mathbf{M}^e = \int_{\Omega_0} \left\{ (\rho h + 2\rho_0)\mathbf{N}^{\mathrm{T}}\mathbf{N} + \left(\frac{\rho^3 h}{12} + \frac{\rho_0 h^2}{2} - \frac{\rho_0 h^2 \nu}{6(1-\nu)} \right) \mathbf{B}_1^{\mathrm{T}}\mathbf{B}_1 \right\} \mathrm{d}x\mathrm{d}y. \tag{46}$$

The global finite element equation for a dynamic analysis is:

$$\mathbf{M}\ddot{\mathbf{r}} + \mathbf{K}\mathbf{r} = \mathbf{f} \tag{47}$$

where $\mathbf{M}$ is the global mass matrix.

Substituting $\mathbf{r}(t) = e^{i\omega t}\mathbf{r}$ in Eq. (47), the natural frequencies and mode shapes can be obtained by solving the following eigenvalue problem:

$$\left[\mathbf{K} - \omega^2 \mathbf{M}\right] \mathbf{r} = \mathbf{0} \tag{48}$$

Table 1 Material properties of aluminum and silicon

Material	E(GPa)	ν	μ_0 (N/m)	λ_0(N/m)	τ_0(N/m)	ρ (kg/m^3)	ρ_0 (kg/m^2)
Al	90	0.23	−0.54251	3.4939	0.5689	2.7×10^3	5.46×10^{-7}
Si	107	0.33	−2.7779	−4.4939	0.6056	2.33×10^3	3.17×10^{-7}

Table 2 Comparison of deflections of simply supported (SSSS) plates under uniformly distributed load obtained from analytical and finite element (FE) methods ($a = 200$ nm, $b = 200$ nm, $h = 10$ nm)

Material	FE solution (quarter model)				Analytical solution
	2 × 2	4 × 4	10 × 10	12 × 12	
Al					
$w(0,0)$	0.03864	0.03735	0.03698	0.03696	0.03690
	(0.04902)	(0.04689)	(0.04628)	(0.04625)	(0.04617)
$w(0.25a,0.25a)$	0.02811	0.02715	0.02688	0.02687	0.02683
	(0.03546)	(0.03392)	(0.03348)	(0.03345)	(0.03339)
Si					
$w(0, 0)$	0.03810	0.03667	0.03627	0.03625	0.03619
	(0.04636)	(0.04418)	(0.04357)	(0.04353)	(0.04344)
$w(0.25a,0.25a)$	0.02769	0.02665	0.02635	0.02633	0.02629
	(0.03354)	(0.03196)	(0.03151)	(0.03148)	(0.03142)

Deflections corresponding to the classical plate theory are shown in parentheses

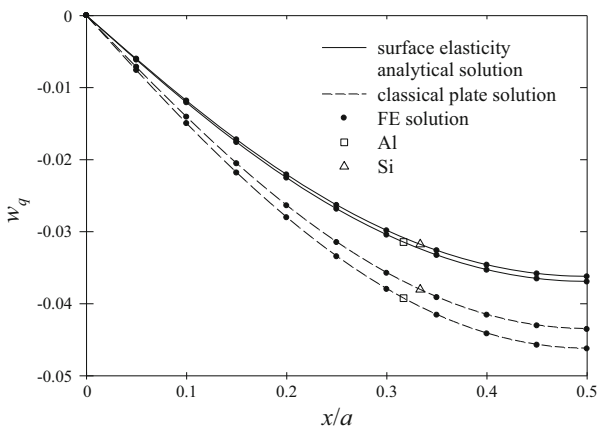

Fig. 2 Deflection profiles of Al and Si plates with all edges simply supported (SSSS) under uniformly distributed load ($a = 200$ nm, $b = 200$ nm, $h = 10$ nm)

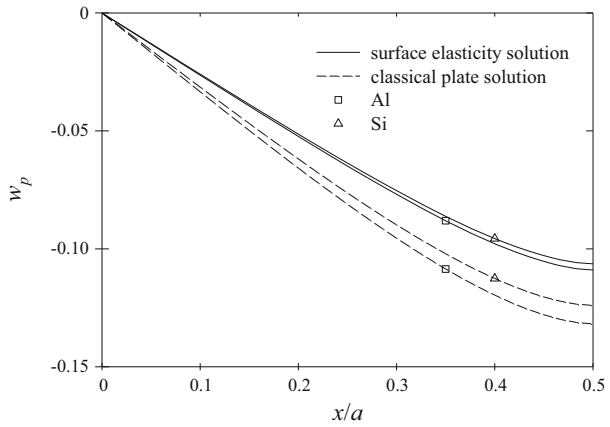

Fig. 3 Deflection profiles of Al and Si plates with all edges simply supported (SSSS) under point load obtained from analytical solutions ($a = 200\,\text{nm}$,b = 200 nm, $h = 10\,\text{nm}$)

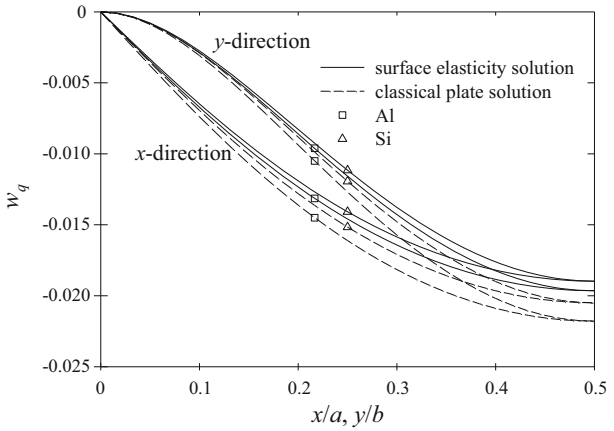

Fig. 4 Deflection profiles of silicon SCSC plates under uniformly distributed load obtained from analytical solutions ($a = 200\,\text{nm}$, $b = 200\,\text{nm}$, $h = 10\,\text{nm}$)

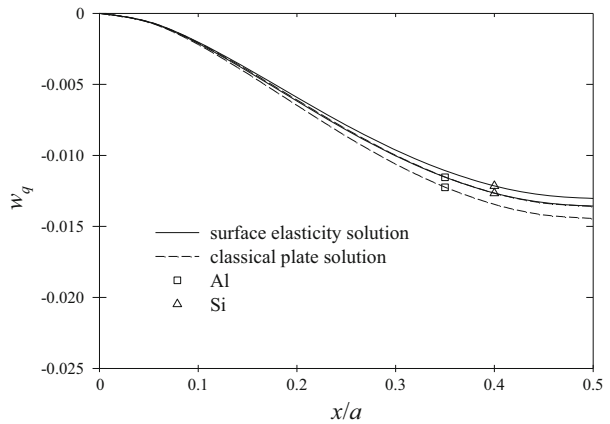

Fig. 5 Deflection profiles of Al and Si plates with all edges clamped (CCCC) under uniformly distributed load obtained from FE solutions ($a = 200\,\text{nm}$, $b = 200\,\text{nm}$, $h = 10\,\text{nm}$)

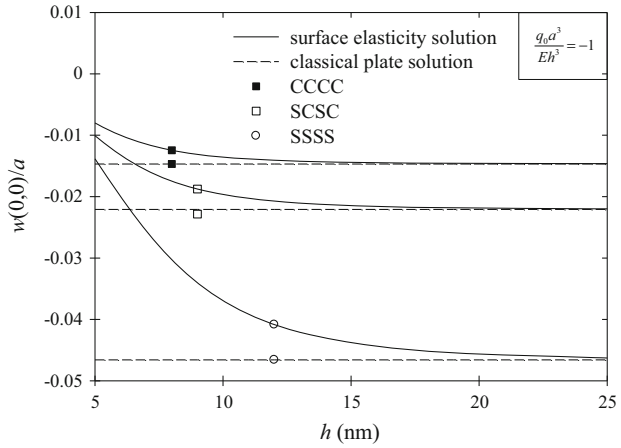

Fig. 6 Size-effect of central deflection of uniformly loaded Al plates with different thicknesses under SSSS, SCSC and CCCC boundary conditions obtained from FE solutions ($a = 200\,\text{nm}$, $b = 200\,\text{nm}$)

where ω is the frequency of vibration in rad/s.

5 Numerical results and discussion

Analytical solutions and the FE formulation presented in the previous sections are implemented in a computer code to examine the influence of various material and geometric parameters as well as boundary conditions on the static and dynamic behaviors of rectangular nanoscale plates. Plates made of aluminum (Al) and silicon (Si) are used in the numerical study. The relevant bulk and surface material properties are given in Table 1 [11,12].

The accuracy of the present analytical and finite element (FE) solutions and the convergence of finite element solutions are first assessed. For this purpose, a plate with all edges simply supported (SSSS) under uniformly distributed loading is considered. Due to the symmetry of the plate geometry and loading, a quarter model with $N \times N$ elements is employed for the finite element analysis. The numerical results for both finite element solutions and analytical solutions are presented in Table 2. The finite element solutions converge and agree within 0.3 % of analytical solutions when the number of plate elements $N \geq 10$. The accuracy of the present solution is also verified by comparing with the limiting case of classical plate theory solutions [15]. The solutions from the current model are obtained for the classical case by setting the surface material coefficients μ_0, λ_0 and τ_0 to zero. These comparisons are not presented in the paper for brevity. Very good agreement between the two sets of solutions is noted.

Next, selected numerical results are presented to investigate the influence of surface properties and boundary conditions on the size-dependent static and free vibration response. Deflection profiles of Si and Al nanoplates with all edges simply supported (SSSS) under a uniformly distributed load (q_0) and a concentrated point load (P_0) at the center of the plate are shown in Figs. 2 and 3, respectively. Deflections of SSSS plates are obtained from analytical solutions presented in Sect. 3. Nondimensional central displacements of the plate, $w_q = w(0,0)Eh^3/(q_0 a^4)$ and $w_P = w(0,0)Eh^3/(P_0 a^2)$, are considered in the numerical study. The solutions for an identical classical plate (zero surface material parameters) [15] are also shown in Figs. 2 and 3 for comparison. These numerical results clearly show that surface energy effects have a significant influence on plate deflections. It is observed that static deflections of Al and Si nanoplates under both types of loading are lower than the corresponding classical plate solutions. This implies that surface energy effects make the plates stiffer compared to the classical plate theory.

Deflection profiles of Al and Si plates with two opposite edges simply supported and the other two edges clamped (SCSC) and plates with all edges clamped (CCCC) are shown in Figs. 4 and 5, respectively. Deflections of SCSC and CCCC plates are obtained from the analytical solutions (Sect. 3) and FEM (Sect. 4), respectively. Similar to a simply supported plate (Fig. 2), the surface energy effect produces stiffening of the plates, but the effect is less prominent. Note that the main contribution from the surface energy is due to the surface residual stress τ_0 and the associated Young–Laplace effect that is directly proportional to the plate curvature. The radius of curvature of a plate with clamped edges is generally higher than that of a simply supported plate. Therefore, the influence of surface residual stress is more prominent for simply supported plates. A similar behavior was also observed for nanobeams [7].

Table 3 Natural frequencies of Al and Si nanoplates for different boundary conditions ($a = 200\,\text{nm}$, $b = 200\,\text{nm}$, $h = 10\,\text{nm}$) obtained from FE solutions

Material	Boundary condition	Natural frequency (GHz)			
		ω_{11}	ω_{22}	ω_{33}	ω_{44}
Al	SSSS	9.242	33.569	74.027	130.656
		(8.451)	(33.805)	(76.061)	(135.220)
	SCSC	13.200	40.452	85.203	135.449
		(12.567)	(40.294)	(86.056)	(137.666)
	CCCC	16.072	45.932	89.540	144.146
		(15.614)	(45.991)	(90.602)	(146.534)
Si	SSSS	11.028	40.574	89.740	158.561
		(10.227)	(40.906)	(92.039)	(163.630)
	SCSC	15.773	48.602	102.503	163.170
		(15.205)	(48.707)	(103.946)	(166.356)
	CCCC	19.258	55.221	107.664	173.122
		(18.890)	(55.578)	(109.331)	(176.504)

Natural frequency from the corresponding classical plate theory is shown in parentheses

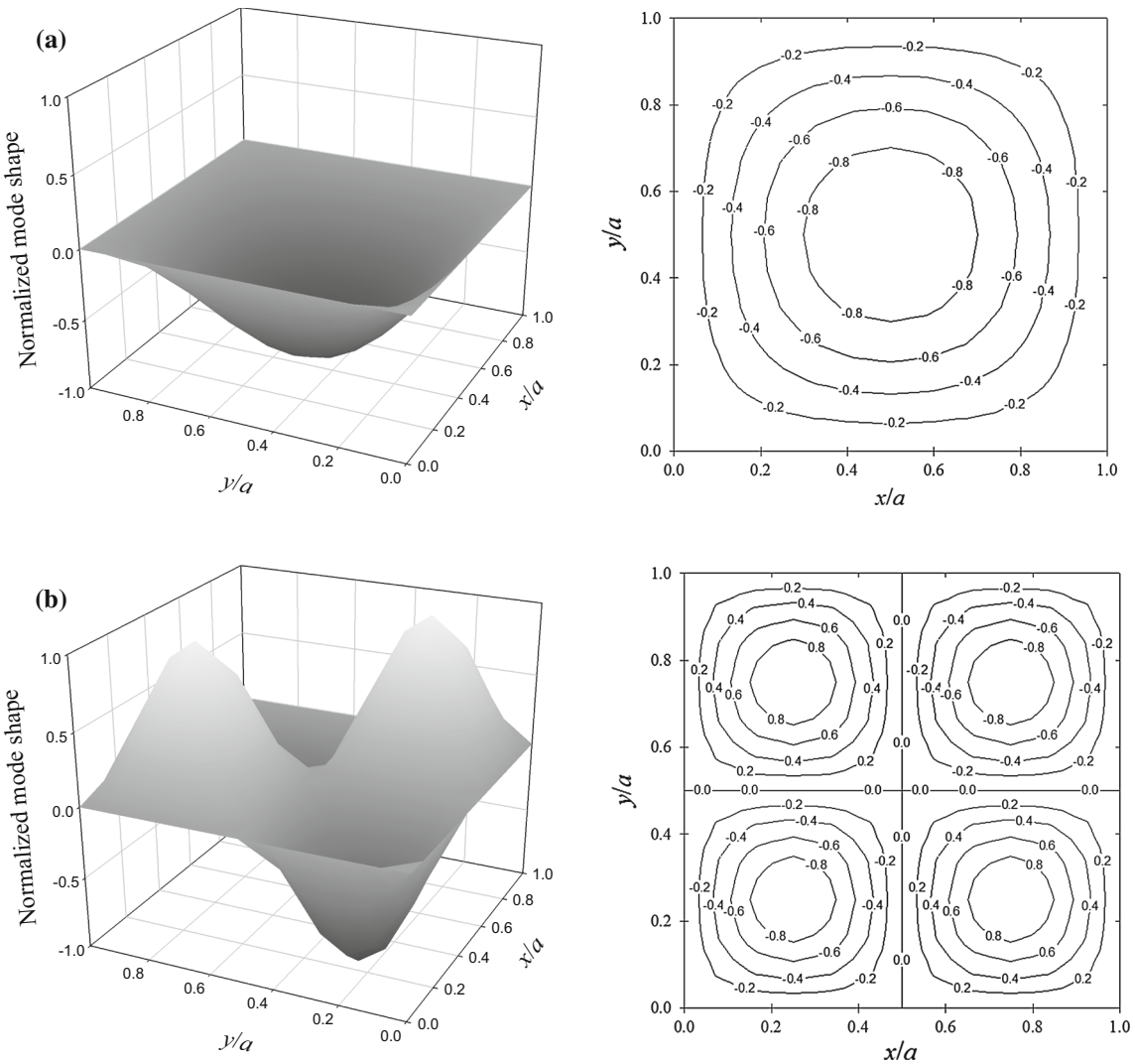

Fig. 7 Mode shapes of SSSS nanoplates obtained from FE solutions **a** first mode and **b** second mode

The size-effect of the response of nanoplates subjected to a uniformly distributed load (q_0) for different boundary conditions is illustrated in Fig. 6. Plates made of aluminum (Al) with $a = 200\,\text{nm}$, $b = 200\,\text{nm}$ and thickness (h) varying from 5 to 25 nm are considered. The solutions presented in Fig. 6 are obtained from the

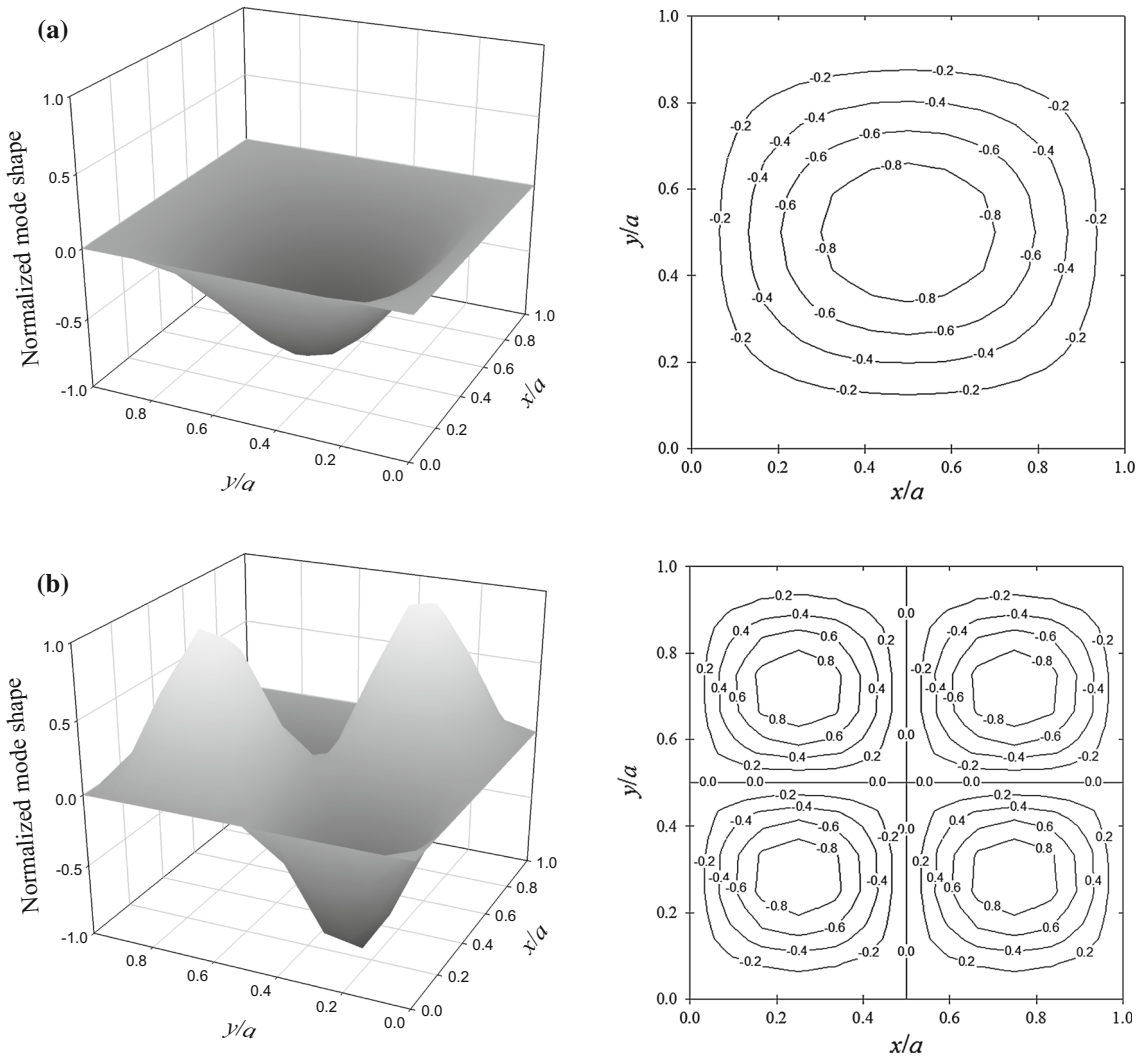

Fig. 8 Mode shapes of SCSC nanoplates obtained from FE solutions **a** first mode and **b** second mode

finite element (FE) model outlined in Sect. 4. The variation of normalized plate deflection, $w(0,0)/a$, where $w(0,0)$ is the deflection at the center of the plate with the plate thickness is plotted in Fig. 6 in which the nondimensional applied load is kept constant for all plates, i.e., $q_0a^3/(Eh^3) = -1$. The classical solutions for the three boundary conditions are identical and independent of the plate thickness for a given nondimensional loading and plate boundary conditions. The size-effect on the normalized deflection compared to the classical case is clearly evident from Fig. 6, and the solutions confirm that the plate behavior significantly depends on the presence of surface residual stress. In addition, the size dependency of the plate response depends on the boundary conditions of the plate. Plates with all edges simply supported (SSSS) show the highest dependency on size followed by SCSC plates and clamped plates (CCCC). Furthermore, the numerical results reveal that the size-effects reduce with increasing plate thickness h. In particular, the size-dependent behavior becomes negligible when the thickness of the plate is >20 nm.

Natural frequencies of Al and Si nanoplates with different boundary conditions, i.e., SSSS, SCSC and CCCC, are presented in Table 3. The corresponding mode shapes of Al plates are depicted in Figs. 7, 8 and 9. These solutions are based on the finite element (FE) model. It is noted that the plate mode shapes are not significantly different from the corresponding classical plate mode shapes. The natural frequencies obtained from the classical plate theory for identical plates are shown in parentheses in Table 3. Table 3 confirms that the surface stress plays an important role on the first (lowest) natural frequency of both Al and Si nanoplates. The effect is more prominent in the case of simply supported boundary conditions (SSSS) when compared to

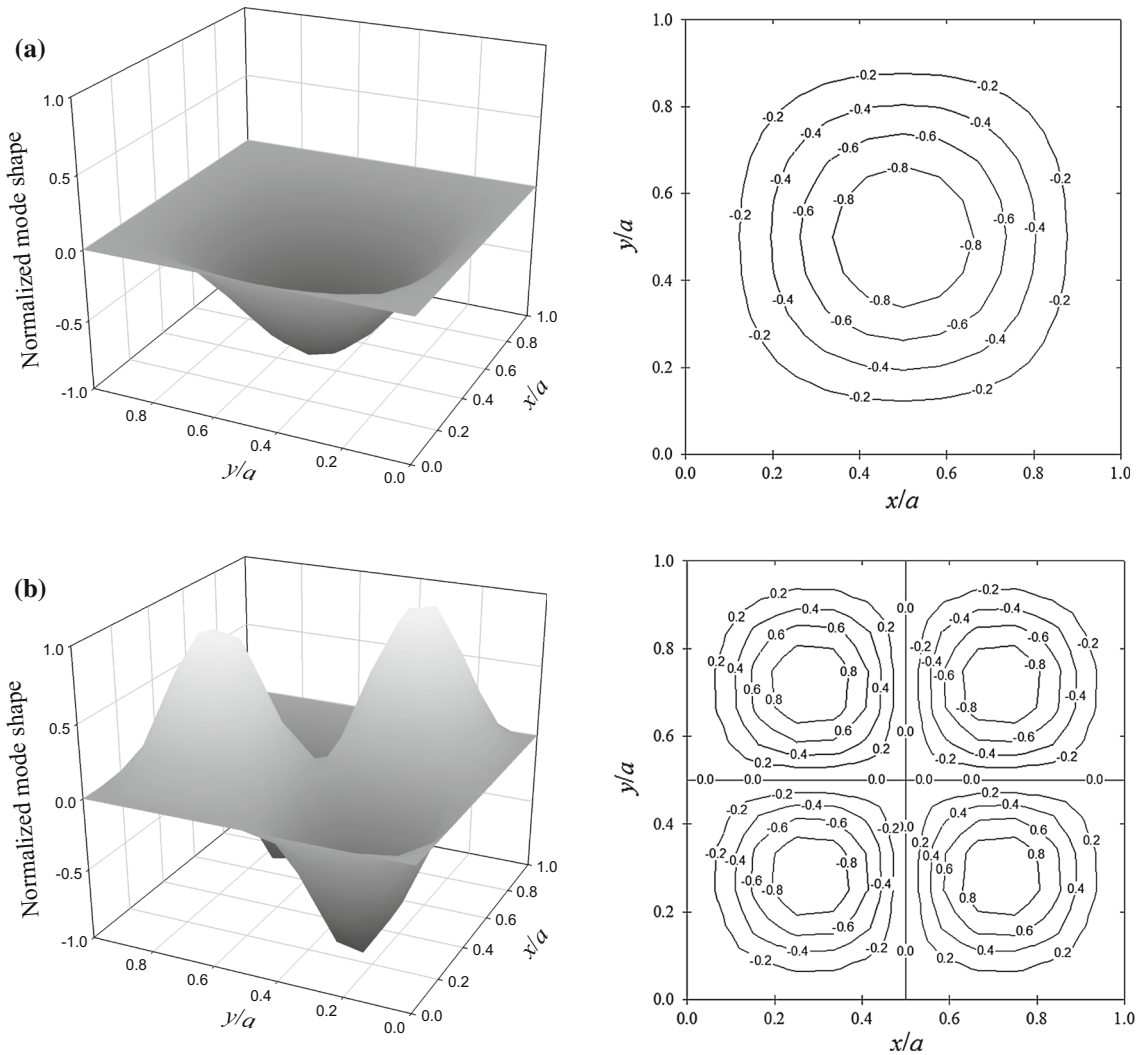

Fig. 9 Mode shapes of CCCC nanoplates obtained from FE solutions **a** first mode and **b** second mode

the cases of CCCC and SCSC plates, similar to the behavior observed for the deflection profiles. The presence of surface stresses leads to higher fundamental natural frequencies for all types of boundary conditions when compared to the corresponding classical plates. This behavior is also consistent with the stiffer response of nanoplates observed in Figs. 2, 3 and 4. It is also observed that the surface effect is less significant on higher natural frequencies, while the classical plate solutions for higher modes are slightly larger than the corresponding nanoplate solutions.

An interpretation of the influence of the surface energy on the natural frequencies cannot be obtained directly from Eq. (32) for arbitrary boundary conditions. However, the analytical solution for natural frequencies of SSSS plates given by Eq. (34) presents some insight into the behavior observed in Table 3. The effect of surface mass density (ρ_0) terms in Eq. (34) is so negligible compared to the bulk mass density terms, and these can be dropped without loss of any accuracy. This simplification results in the following approximation for natural frequencies of SSSS plates:

$$\omega_{mn}^2 \cong \frac{D^*\left(\lambda_m^2+\lambda_n^2\right)}{\left(\frac{\rho h}{\lambda_m^2+\lambda_n^2}+\frac{\rho^3 h}{12}\right)}+\frac{2\tau_0}{\left(\frac{\rho h}{\lambda_m^2+\lambda_n^2}+\frac{\rho^3 h}{12}\right)}. \tag{49}$$

Note that the denominator of Eq. (49) is primarily influenced by the second term (constant) as the first term rapidly becomes smaller with increasing m and n (higher modes). The second term of Eq. (49) therefore reflects

a direct contribution of surface residual stress (the key parameter of surface energy effects), and it is nearly constant for all modes. The first term of Eq. (49) increases with increasing m and n (D^* is constant for a given plate and dominated by the bulk bending stiffness compared to the contributions from surface effects) and controls the magnitude of natural frequency, while the second term becomes relatively smaller compared to the first term for higher frequencies. This is the reason for diminishing influence of surface effects for higher natural frequencies observed in Table 3.

6 Conclusions

A new mechanistic model based on the Gurtin–Murdoch surface elasticity theory is developed to analyze rectangular nanoplates. It is found that closed-form analytical solutions can be derived for certain plate configurations. A finite element formulation for nanoplates is successfully developed based on the weighted residual method. Numerical results indicate that the static and dynamic responses are significantly influenced by surface energy effects and plate boundary conditions. The highest influence of the surface energy effect is observed for simply supported plates followed by SCSC plates, and only minor effects are noted for clamped plates. This behavior is consistent with the fact that the surface stress contribution associated with the Young–Laplace effect is controlled by the curvature of the plate. Plates with smaller radius of the curvature (simply supported) therefore show the highest effect of surface stress. The first natural frequency of plates shows a substantial effect of surface stress, but the influence diminishes for higher natural frequencies. However, mode shapes show negligible influence of surface energy effects.

Acknowledgments The work presented in this paper was supported by Grants for New Researcher from Thailand Research Fund and Mahidol University (TRG5780139), and Natural Sciences and Engineering Research Council of Canada.

References

1. Craighead, H.G.: Nanoelectromechanical systems. Science **290**, 1532–1535 (2000)
2. Miller, R.E., Shenoy, V.B.: Size-dependent elastic properties of nanosized structural elements. Nanotechnology **11**, 139–147 (2000)
3. Gurtin, M.E., Murdoch, A.I.: A continuum theory of elastic material surfaces. Arch. Ration. Mech. Anal. **57**, 291–323 (1975)
4. Gurtin, M.E., Murdoch, A.I.: Addenda to our paper: a continuum theory of elastic material surfaces. Arch. Ration. Mech. Anal. **59**, 389–390 (1975)
5. He, L.H., Lim, C.W., Wu, B.S.: A continuum model for size-dependent deformation of elastic films of nano-scale thickness. Int. J. Solids Struct. **41**, 847–857 (2004)
6. He, J., Lilley, C.M.: Surface effect on the elastic behavior of static bending nanowires. Nano Lett. **8**, 1798–1802 (2008)
7. Liu, C., Rajapakse, R.K.N.D.: Continuum models incorporating surface energy for static and dynamic response of nanoscale beams. IEEE Trans. Nanotechnol. **9**, 422–431 (2010)
8. Sapsathiarn, Y., Rajapakse, R.K.N.D.: A model for large deflections of nanobeams and experimental comparison. IEEE Trans. Nanotechnol. **11**, 247–254 (2012)
9. Liu, C., Rajapakse, R.K.N.D.: A size-dependent continuum model for nanoscale circular plates. IEEE Trans. Nanotechnol. **12**, 13–20 (2013)
10. Sapsathiarn, Y., Rajapakse, R.K.N.D.: Finite-element modeling of circular nanoplates. J. Nanomech. Micromech. ASCE **3**, 59–66 (2013)
11. Miller, R.E., Shenoy, V.B.: Size-dependent elastic properties of nanosized structural elements. Nanotechnology **11**, 139–147 (2000)
12. Shenoy, V.B.: Atomistic calculations of elastic properties of metallic fcc crystal surfaces. Phys. Rev. B **71**, 094104–109410411 (2005)
13. Levy, M.: Sur L'equilibrie Elastique D'une Plaque Rectangulaire. Comptes Rendues Academie Des Sciences **129**, 535–539 (1899)
14. Zienkiewicz, O.C., Taylor, R.L.: The Finite Element Method, 5th edn. Butterworth-Heinemann, Boston (2000)
15. Timoshenko, S.P., Woinowsky-Krieger, S.: Theory of Plates and Shells. McGraw Hill, New York (1959)

Manuscript

Mechanistic Models and Variational Formulation of Nano-scale Beam Bending

Y. Sapsathiarn[a] and R.K.N.D. Rajapakse[b]

[a] Department of Civil and Environmental Engineering, Mahidol University, Nakornpathom, Thailand

[b] Department of Civil and Environmental Engineering, Carleton University, Ottawa, Canada K1S 5B6

(Submitted to ***NANO LETTERS***)

ABSTRACT— In this Letter, a variational approach is used to study bending of nanoscale beams with surface energy effects. This work is motivated by the differences that exist between recently reported solutions for nano-cantilevers. Surface energy is incorporated using Gurtin-Murdoch surface elasticity theory. The governing equation and admissible boundary conditions are obtained from a variational formulation. Closed-form analytical solutions for beams with different boundary conditions, i.e., simply-supported, cantilevered, and clamped-clamped ends, are re-examined and the reason for differences between existing solutions for nano-cantilevers is identified.

KEYWORDS: Nanoscale beams, size dependent behavior, mechanistic model, nanoelectromechanical systems, surface residual stress, variational methods

1. Introduction

Nanobeams are used in a wide range of nanotechnology devices (e.g., resonators and sensors). Several past studies have developed mathematical models for the mechanical response of nanobeams. He and Lilley (2008) applied the Gurtin-Murdoch continuum theory (Gurtin and Murdoch, 1975a and 1975b) to develop a mathematical model for nanobeams. They concluded that the effect of residual surface tension can be considered equivalent to a distributed loading and nanobeams can be modeled by the classical beam theory with a modified bending stiffness. The solutions given by He and Lilley (2008) showed that a cantilever nanobeam is softer whereas a simply-supported or fixed-fixed nanobeam is stiffer compared to a classical beam when the surface residual stress is positive (Fig. 1).

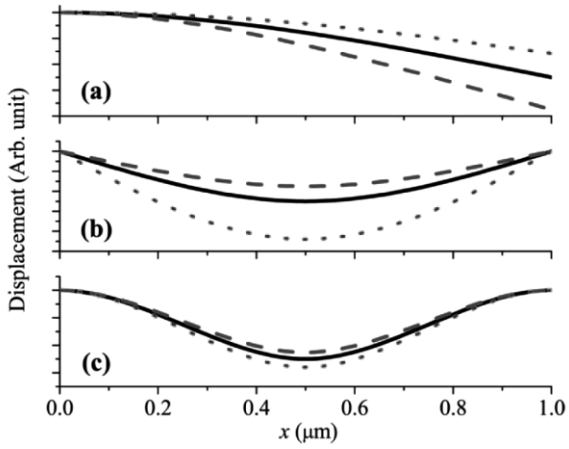

Figure 1. [*reproduced*] Deflections of nanobeams as per He and Lilley (2008) (a) cantilever, (b) simply supported, (c) fixed-fixed; solid line: $\tau_0 = 0$; dashed line; $\tau_0 = +1$ μN/μm; and dotted line: $\tau_0 = -1$ μN/μm.

This behaviour was explained by considering the sign of beam curvature under different end conditions. Liu and Rajapakse (2010) also developed a mathematical model for nanobeams based on the Gurtin-Murdoch theory and used the equilibrium of an infinitesimal

beam element and full elastic field to derive their model. However, their solutions show that cantilever, simply-supported and fixed-fixed beams are stiffer compared to the corresponding classical beams under positive surface residual stress. The objective of this Letter is to investigate this discrepancy. The governing equation and admissible boundary conditions are re-derived using a variational method. The root cause of the discrepancy is identified.

2. Variational Formulation

Consider a thin beam with cross-section symmetric about the z-axis and length L as shown in Fig. 2. A beam based on the Gurtin-Murdoch continuum model has an elastic surface (mathematically zero thickness) perfectly bonded to the bulk material. The outward unit normal n and tangent t of the cross-section are as shown in Fig. 2. The elastic surface has distinct material properties and accounts for the surface energy effects (Miller and Shenoy, 2000; Lee and Rudd, 2007).

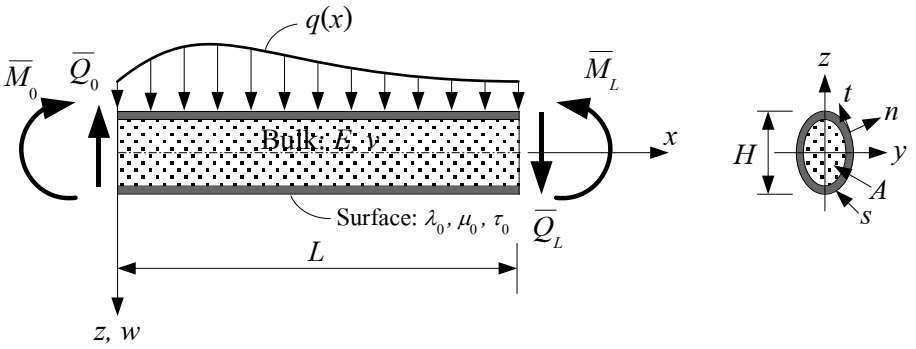

Figure 2. Geometry of beam and coordinate system.

Let w denote the deflection along the centroidal axis $(x,0,0)$ of the beam. For thin beams with Euler-Bernoulli hypothesis, the displacements u_x and u_z along the x- and z- directions are given by:

$$u_x = -z\frac{\partial w(x,t)}{\partial x};\quad u_z = w(x,t) \tag{1}$$

Therefore, the non-zero bulk strain is:

$$\varepsilon_{xx} = \frac{\partial u_x}{\partial x} = -z\frac{\partial^2 w(x,t)}{\partial x^2} \tag{2}$$

The beam is in the plane stress state with non-zero bulk stresses, σ_{xx} and σ_{zz}. The elastic surface (outward unit normal n) has non-zero stresses τ_{xx} and τ_{nx}. Assuming a homogeneous and isotropic bulk material, the relevant constitutive relations of the bulk can be expressed as,

$$\sigma_{xx} = E\varepsilon_{xx} + \nu\sigma_{zz} \tag{3}$$

where E is the elastic modulus and ν is Poisson's ratio.

The stress component σ_{zz} is usually neglected in the classical beam theory. However, the Young-Laplace condition (Young, 1805; Laplace, 1805; Chen et al., 2006) along the surface-bulk interface requires a non-zero σ_{zz}. Following Lu et al. (2006), σ_{zz} is assumed to vary linearly through the beam thickness to satisfy the equilibrium conditions on the interface. Therefore,

$$\sigma_{zz} = \frac{1}{2}(\sigma_{zz}^{+} + \sigma_{zz}^{-}) + \frac{z}{H}(\sigma_{zz}^{+} - \sigma_{zz}^{-}) \tag{4}$$

where σ_{zz}^{+} and σ_{zz}^{-} are stresses at the top and bottom fibers, respectively, and H is the height of the beam.

The surface constitutive relations can be expressed as (Gurtin and Murdoch, 1975a and 1975b),

$$\tau_{xx} = \tau_0 + (2\mu_0 + \lambda_0)u_{x,x}; \quad \tau_{nx} = \tau_0 u_{n,x} \tag{5}$$

where τ_0 is the surface residual stress under unconstrained conditions; μ_0 and λ_0 are surface Lame constants; and u_x and u_n are the displacements along the *x*- and *n*- direction respectively.

The surface equilibrium at any point is expressed by (Gurtin and Murdoch, 1975a and 1975b),

$$\tau_{zx,x} - \sigma_{zz} n_z = \rho_0 \ddot{u}_z^s \tag{6}$$

where $\ddot{u}_z^s$ denotes the acceleration of surface layer in the *z*-direction.

By substituting eqs (1), (2) and (6) into eqs (3), (4) and (5), the following expressions for non-zero stresses are obtained.

$$\sigma_{zz} = \frac{2z}{H}(\tau_0 \frac{\partial^2 w}{\partial x^2} - \rho_0 \ddot{w}); \quad \sigma_{xx} = -Ez\frac{\partial^2 w}{\partial x^2} + \frac{2\nu z}{H}\left(\tau_0 \frac{\partial^2 w}{\partial x^2} - \rho_0 \ddot{w}\right) \tag{7}$$

$$\tau_{xx} = \tau_0 - z(2\mu_0 + \lambda_0)\frac{\partial^2 w}{\partial x^2}; \quad \tau_{nx} = \tau_0 \frac{\partial w}{\partial x} n_z \tag{8}$$

The total strain energy of the beam contains two parts, i.e., the elastic strain energy stored in the bulk material (U^B) and the elastic strain energy of the surface (U^s):

$$U^B = \frac{1}{2}\int_V \sigma_{xx}\varepsilon_{xx} dV \;;\; U^s = \frac{1}{2}\int_\Gamma (\tau_{xx}\varepsilon_{xx} + \tau_{nx}\varepsilon_{nx}) d\Gamma \tag{9}$$

where V is the bulk volume and Γ is the surface area.

From eqs (7), (8) and (9), the strain energies stored in the bulk and surface can be expressed as,

$$U^B = \frac{1}{2}\left(EI - \frac{2\nu I\tau_0}{H}\right)\int_0^L \left(\frac{\partial^2 w}{\partial x^2}\right)^2 dx + \frac{2\nu I\rho_0}{H}\int_0^L \ddot{w}\left(\frac{\partial^2 w}{\partial x^2}\right) dx \tag{10}$$

$$U^s = \frac{1}{2}(2\mu_0 + \lambda_0) I^* \int_0^L \left(\frac{\partial^2 w}{\partial x^2}\right)^2 dx + \frac{1}{2}\tau_0 s^* \int_0^L \left(\frac{\partial w}{\partial x}\right)^2 dx \tag{11}$$

where $I = \int_A z^2 dA$ is the moment of inertia of the beam cross-section; $I^* = \int_s z^2 ds$ is the perimeter moment of inertia; $s^* = \int_s n_z^2 ds$; A is the cross-sectional area and s is the perimeter of the cross section.

In the case of beams with rectangular cross-section of height $2h$ and width b, the geometry parameters are given as,

$$I = \frac{2bh^3}{3};\; I^* = 2bh^2 + \frac{4h^3}{3};\; s^* = 2b \text{ and } H = 2h \tag{12}$$

The potential energy due to a distributed load $q(x)$ on the beam, prescribed end moment ($\bar{M}$) and end force ($\bar{Q}$), as shown in Fig.2, is

$$V = -\int_0^L q(x)w(x)dx + \left(\bar{M}\frac{\partial w}{\partial x}\right)\Big|_0^L - \left(\bar{Q}w\right)\Big|_0^L \tag{13}$$

where $\bar{M}$ and $\bar{Q}$ are the moment and force at the ends of the beam respectively.

The kinetic energy of nanoscale beam is,

$$T = \frac{1}{2}\int_0^L \rho A(\dot{w})^2 dx + \frac{1}{2}\int_0^L \rho_0 s^* (\dot{w})^2 dx \tag{14}$$

In view of eqs , (10), (11), (13) and (14), the total energy functional of nanoscale beam is,

$$\begin{aligned}\Pi(x, w, w', w'') &= U^B + U^s + V + T \\ &= \frac{1}{2}\left[EI - \frac{2\nu I\tau_0}{H} + (2\mu_0 + \lambda_0)I^*\right]\int_0^L \left(\frac{\partial^2 w}{\partial x^2}\right)^2 dx + \frac{1}{2}\tau_0 s^* \int_0^L \left(\frac{\partial w}{\partial x}\right)^2 dx \\ &\quad + \frac{2\nu I\rho_0}{H}\int_0^L \ddot{w}\left(\frac{\partial^2 w}{\partial x^2}\right)dx + \frac{1}{2}\int_0^L \rho A(\dot{w})^2 dx + \frac{1}{2}\int_0^L \rho_0 s^* (\dot{w})^2 dx \\ &\quad - \int_0^L q(x)w(x)dx + \left(\bar{M}\frac{\partial w}{\partial x}\right)\Big|_0^L - \left(\bar{Q}w\right)\Big|_0^L \end{aligned} \tag{15}$$

Taking the variation of eq (15) together with integration by parts leads to the following governing equation for a beam (Washizu, 1982):

$$\begin{aligned}&\left[EI - \frac{2\nu I\tau_0}{H} + (2\mu_0 + \lambda_0)I^*\right]\frac{\partial^4 w}{\partial x^4} - \tau_0 s^* \frac{\partial^2 w}{\partial x^2} - q \\ &\qquad = -\frac{2\nu I\rho_0}{H}\frac{\partial^4 w}{\partial x^2 \partial t^2} - (\rho A + \rho_0 s^*)\frac{\partial^2 w}{\partial t^2}, \quad 0 < x < L \end{aligned} \tag{16}$$

and the admissible boundary conditions for a nanoscale beam are:

$$\bar{Q} = -\left[EI - \frac{2\nu I\tau_0}{H} + (2\mu_0 + \lambda_0)I^*\right]\left(\frac{\partial^3 w}{\partial x^3}\right) + \tau_0 s^* \frac{\partial w}{\partial x} - \frac{2\nu I\rho_0}{H}\frac{\partial^3 w}{\partial x \partial t^2} \quad \text{or} \quad w = \bar{w} \tag{17}$$

$$\bar{M} = -\left[EI - \frac{2\nu I \tau_0}{H} + (2\mu_0 + \lambda_0) I^* \right] \left(\frac{\partial^2 w}{\partial x^2} \right) - \frac{2\nu I \rho_0}{H} \frac{\partial^2 w}{\partial t^2} \qquad \text{or} \quad \frac{\partial w}{\partial x} = \bar{w}' \qquad (18)$$

where $\bar{w}$ and $\bar{w}'$ denote the prescribed displacement and slope at the beam end respectively.

Equation (16) is similar to the classical beam equation but includes an additional term due to the effect of residual surface stress. It reduces to the classical model (Gere and Timoshenko, 1991) if the surface energy effect is completely neglected, i.e., μ_0, λ_0 and τ_0 are zero. Equations (16) - (18) are identical to the corresponding equations derived by Liu and Rajapakse (2010) using the force and moment equilibrium of an infinitesimal beam element. Based on eq (16), the modified bending stiffness of nanobeam can be defined as,

$$K_b^* = EI - \frac{2\nu I \tau_0}{H} + (2\mu_0 + \lambda_0) I^* \qquad (19)$$

The homogeneous solution of eq (16) can be written as,

$$w(x) = C_1 e^{\sqrt{\varepsilon} x} + C_2 e^{-\sqrt{\varepsilon} x} + C_3 x + C_4 \qquad (20)$$

where $\varepsilon = \tau_0 s^* / K_b^*$; K_b^* is defined by eq (19); and C_1 to C_4 are unknown arbitrary constants to be determined from the boundary conditions.

3. Examination of the discrepancy between existing solutions

3.1 He and Lilley Model

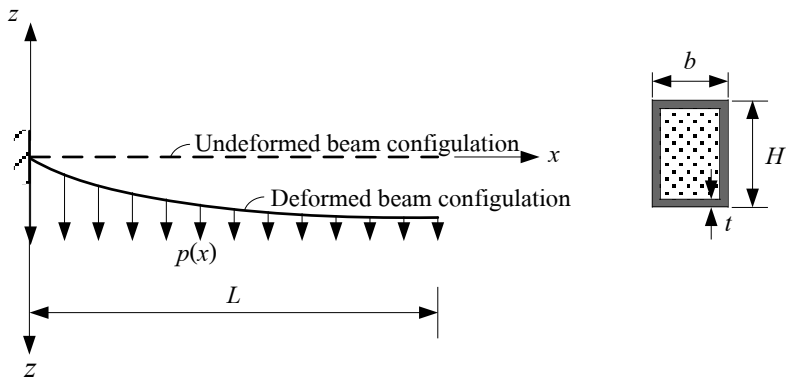

Figure 3. Nanobeam model of He and Lilley (2008).

Consider the solution developed by He and Lilley (2008) for the beam shown in Fig. 3. They derived the governing equation by simply adding an equivalent distributed loading due to surface residual stress (Young-Laplace effect) to the classical beam equation with a modified beam stiffness. Their governing equation is,

$$K_b^{**}\frac{d^4w}{dx^4} = p(x) \tag{21}$$

and in the absence of any applied distributed loading, $p(x)$ was defined by He and Lilley (2008) as

$$p(x) = 2(\tau_0 + E_s\varepsilon_x)b\frac{d^2w}{dx^2} \tag{22}$$

where E_s is the surface elastic modulus, ε_x is the longitudinal surface strain and b is the beam width.

The modified bending stiffness of a rectangular beam K_b^{**} was determined by adding the stiffness contributions of surface layer with thickness *t* and bulk material (Fig. 3). Assuming $t \ll H$, He and Lilley (2008) expressed the stiffness of nanoscale beam by

$$K_b^{**} = EI_1 + \frac{1}{2}E_s bH^2 + \frac{1}{6}E_s H^3 \tag{23}$$

where $I_1 = \frac{1}{12}bH^3$.

By neglecting the contribution due to longitudinal surface strain in $p(x)$, the beam governing equation (21) was simplified to:

$$K_b^{**}\frac{d^4w}{dx^4} \cong 2\tau_0 b\frac{d^2w}{dx^2} \tag{24}$$

which can be re-written as

$$\left[EI + \frac{1}{2}E_s bH^2 + \frac{1}{6}E_s H^3\right]\frac{d^4w}{dx^4} - \tau_0 s^*\frac{d^2w}{dx^2} = 0 \tag{A-1}$$

where $s^* = 2b$.

The above governing equation derived by He and Lilley (2008) is similar to the (static) results of Liu and Rajapakse (2010) and the present variational approach (see eq (16)), except that the modified beam stiffness is different. He and Lilley (2008) obtained the modified bending stiffness by simply adding the contribution of classical bending stiffness of the bulk and that due to a surface layer with finite thickness. However, the nanobeam stiffness given in the present formulation and Liu and Rajapakse (2010) are obtained based on the consideration of full elastic field based on the continuum model of Gurtin-Murdoch.

Moreover, to satisfy the Gurtin-Murdoch surface equilibrium equations, the vertical bulk stress was also considered by Liu and Rajapakse (2010) and in the present formulation. The influence of bulk vertical stress on the bending stiffness is represented by the second term of eq (16).

The homogeneous solutions of the governing equation of He and Lilley (2008) is also given by eq (20) with K_b^* (eq 19)) replaced by K_b^{**} (eq 23)). In the ensuing sections, beams under different end conditions, i.e., simply-supported, cantilevered, and clamped-clamped, are re-examined to identify the reason for the discrepancy between the Liu and Rajapakse (2010) and He and Lilley (2008).

3.2 Beams under different end conditions

3.2.1 Cantilever beams

Consider a cantilever beam of length L subjected to a concentrated static load $\bar{F}_L$ at the free end. According to the present scheme and Liu and Rajapakse (2010), eq (16) governs the (static response) beam and the boundary conditions are expressed by eqs (17) and (18) (by removing the dynamic term). Table 1 compares the boundary conditions used by Liu and Rajapakse (2010) and those used by He and Lilley (2008).

Table 1. Comparison of boundary conditions for cantilever beams.

Liu and Rajapakse (2010)	He and Lilley (2008)
1) $w(0) = 0$	1) $w(0) = 0$
2) $w'(0) = 0$	2) $w'(0) = 0$
3) $M^*(L) = 0$	3) Moment equilibrium at $x = 0$
4) $Q^*(L) = \bar{F}_L$	4) Vertical force equilibrium at $x = 0$

For a static problem, eq (16) is simplified to

$$K_b^* \frac{d^4 w}{dx^4} - \tau_0 s^* \frac{d^2 w}{dx^2} - q = 0 \tag{A-2}$$

and the corresponding natural boundary conditions are

$$\bar{Q} = -K_b^* \frac{d^3 w}{dx^3} + \tau_0 s^* \frac{dw}{dx} \quad \text{and} \quad \bar{M} = -K_b^* \frac{d^2 w}{dx^2} \tag{A-3}$$

The first and second boundary conditions are identical between the two models (see Table 1). In view of eqs (17) and (18), the third and fourth boundary conditions given by Liu and Rajapakse (2010) yield,

$$K_b^* w''(L) = 0 \quad \text{and} \quad -K_b^* w'''(L) + \tau_0 s^* w'(L) = \bar{F}_L \tag{25}$$

Using the first two boundary conditions of Table 1 and eq (25) together with eq (20), the solution for cantilever beam can be obtained as,

$$w(x) = \frac{\bar{F}_L}{K_b^* \varepsilon}\left[x - \frac{\sinh(x\sqrt{\varepsilon} - L\sqrt{\varepsilon}) + \sinh(L\sqrt{\varepsilon})}{\sqrt{\varepsilon}\cosh(L\sqrt{\varepsilon})} \right] = \Omega f(x) \tag{26}$$

where Ω is a constant that depends on the magnitude of load, beam bending stiffness and surface residual stress; and $f(x)$ is a deflection shape function.

Instead of using boundary conditions at the beam ends to determine nanobeam solutions, He and Lilley (2008) replaced the third and the forth boundary conditions by the moment and force equilibrium conditions at $x=0$ (see Table 1). Using the resultant shear force and bending moment of a nanobeam cross section defined in eqs (17) and (18) /or (A-3) together with the condition of zero slope at $x=0$, the moment and vertical force equilibrium at $x=0$ can be written as

$$-K_b^{**}w''(0) \;=\; -\bar{F}_L L \;\text{ and }\; -K_b^{**}w'''(0) \;=\; \bar{F}_L \tag{27}$$

The moment equilibrium condition at the beam end (x = 0) in Table 1 was, however, expressed by He and Lilley (2008) as,

$$K_b^{**}w''(0) \;=\; \bar{F}_L L \;+\; \int_0^L \tau_0 s^* w''\, x\, dx \;=\; \bar{F}_L L \;+\; \tau_0 s^* \left[L w'(L) - w(L) \right] \tag{28}$$

and the force equilibrium at x = 0 was given by He and Lilley (2008) as,

$$-K_b^{**}w'''(0) \;=\; \bar{F}_L \;+\; \int_0^L \tau_0 s^* w''\, dx \;=\; \bar{F}_L \;+\; \tau_0 s^* w'(L) \tag{29}$$

Substitution of the first two boundary conditions of Table 1 and eqs (28) and (29) in the general solution of eq (20) yields the following solution for a cantilever beam based on the He and Lilley (2008) model:

$$w(x) \;=\; \frac{\bar{F}_L \cosh(L\sqrt{\varepsilon})}{K_b^{**}\varepsilon}\left[x - \frac{\tanh(L\sqrt{\varepsilon})}{\sqrt{\varepsilon}} - \frac{\sinh(x\sqrt{\varepsilon} - L\sqrt{\varepsilon})}{\sqrt{\varepsilon}\cosh(L\sqrt{\varepsilon})} \right] \tag{30}$$

Obviously, the solutions given by eqs (26) and (30) are different. To identify the reason for this difference we examine the boundary conditions of the He and Lilley model shown in Table 1. Note that in writing right hand side of eqs (28) and (29), He and Lilley (2008) assumed that a distributed load of magnitude $2b\tau_0 w''$ is acting on the beam by interpreting the right hand side of eq (24) as an equivalent distributed load. Furthermore, they used the expressions for stress resultants of a classical beam in the left hand side of eq (28) and (29) in applying the boundary conditions. As shown here the stress resultants and natural boundary conditions for a Gurtin-Murdoch beam governed by eq (16) are given by eqs (17) and (18). Therefore, the expressions for a classical beam stress resultants used by He and Lilley to derive their solutions are not valid for a Gurtin-Murdoch beam although the governing equations of both schemes are similar [eq (16) and eq (24) respectively]. It is also noted that even though one could interpret the right hand side of eq (24) as equivalent to a load, it is not a physical load. This term fundamentally alters the beam governing equation as it is a function of the beam curvature and results in substantially different stress resultants and natural boundary conditions.

Based on eq (30), He and Lilley (2008) concluded that the cantilever nanobeam exhibits a softer elastic behaviour for $\tau_0 > 0$ as shown in Figure 1(a). They explained that the stiffer or softer behaviour of nanoscale beams is attributed to the signs of the curvature and surface stress during the static bending. The downward curvature for the cantilever nanobeams (Figure 1(a)) results in a positive curvature and, according to eq (24), a positive curvature results in a positive distributed transverse force in the same direction with the external load if $\tau_0 > 0$. Thus, the distributed transverse force increases the transverse displacement of the beam bending and the cantilever nanobeams behaves like a softer material.

The explanation of softer and stiffener behaviour of nanoscale beams using the equivalent transverse distributed force (eq (24)) and the signs of the curvature is questionable. Consider the governing equation of nanobeam in eq (16) / (A-2), it could be seen that the differentiation of nanobeam bending from the classical beam bending is due to the modified bending stiffness $EI - 2\nu I\tau_0 / H + (2\mu_0 + \lambda_0)I^*$ and the presence of the second order derivative term $-\tau_0 s^* d^2 w / dx^2$. Similar to the case of column buckling, the second order derivative term alter the structure of the nanobeam governing equation considerably and is primarily responsible for the diversity of nanoscale beam behaviour from the classical beam. The interpretation of second order derivative term as a distributed force along the nanoscale beam is questionable.

We also note that the *general solutions* for beam deflection are identical for He and Lilly (2008) and Liu and Rajapakse (2010) (see eq (20)). Therefore, it can be concluded that as long as the boundary conditions are expressed in terms of deflections, slopes, bending moment and/or shear force at a cross section with zero slope, the solutions obtained from He and Lilley (2008) and Liu and Rajapakse (2010) are identical. We prove this by considering the case of simply-supported and fixed-fixed beams in the next sections.

3.2.2 Simply-supported beam

Table 2 summarizes the boundary conditions for a simply supported beam employed by He and Lilley (2008) and Liu and Rajapakse (2010). As the beam structure is symmetric with respect to the loading plane, the half beam model $(0 \le x \le L/2)$ can be used in the analysis.

Table 2. Comparison of boundary conditions for simply supported beams.

Liu and Rajapakse (2010)	He and Lilley (2008)
1) $w(0) = 0$	1) $w(0) = 0$
2) $M^*(0) = 0$	2) $w''(0) = 0$
3) $w'(L/2) = 0$	3) $w'(L/2) = 0$
4) $Q^*(L/2) = \dfrac{\bar{F}_L}{2}$	4) Force equilibrium at $x = 0$

In view of eq (17) / (A-3), the second boundary condition of Liu and Rajapakse [$M^*(0) = 0$] leads to $w''(0) = 0$. Therefore the first three boundary conditions of He and Lilley (2008) given in Table 2 is identical to Liu and Rajapakse (2010). Next, the substitution of the forth boundary condition of Liu and Rajapakse ($Q^*(L/2) = \bar{F}_L / 2$) together with $w'(L/2) = 0$ in eq (17) yields,

$$-K_b^* w'''(L/2) = \frac{\bar{F}_L}{2} \tag{31}$$

Based on eq (A-3), the forth boundary condition in Table 2 given by He and Lilley (2008), i.e., force equilibrium at $x = 0$, can be written as,

$$-K_b^{**} w'''(0) + \tau_0 s^* w'(0) = \frac{\bar{F}_L}{2} \tag{32}$$

The forth boundary condition was considered by He and Lilley (2008) as

$$-K_b^{**} w'''(0) = \frac{\bar{F}_L}{2} + \int_0^{L/2} \tau_0 s^* w'' \, dx = \frac{\bar{F}_L}{2} - \tau_0 s^* w'(0) \tag{33}$$

It can be seen that eq (33) is identical to eq (32). It is also found that the solutions for simply-supported beams from the two approaches are identical. The solution for deflection of a simply-supported beam is given by

$$w(x) = \frac{\bar{F}_L}{2K_b^*\varepsilon}\left[x - \frac{\sinh(x\sqrt{\varepsilon})}{\sqrt{\varepsilon}\cosh(L\sqrt{\varepsilon}/2)}\right] \tag{34}$$

3.2.3 Clamped-clamped beam

Table 3 summarizes the boundary conditions for a clamped-clamped beam used by He and Lilley (2008) and Liu and Rajapakse (2010). The half beam model $(0 \le x \le L/2)$ is used in the analysis due to symmetry of the beam structure with respect to the loading plane.

Table 3. Comparison of boundary conditions for clamped-clamped beams.

Liu and Rajapakse (2010)	He and Lilley (2008)
1) $w(0) = 0$	1) $w(0) = 0$
2) $w'(0) = 0$	2) $w'(0) = 0$
3) $w'(L/2) = 0$	3) $w'(L/2) = 0$
4) $Q^*(L/2) = \frac{\bar{F}_L}{2}$	4) Force equilibrium at $x = 0$

The first three boundary conditions are identical. The forth boundary conditions for Liu and Rajapakse (2010) and He and Lilley (2008) beam models are given in eqs (31) and (33) respectively. It can be shown that the two models again result in identical solutions for clamped-clamped beams. The solution for deflection of a clamped-clamped beam is obtained as

$$w(x) = \frac{\bar{F}_L}{2K_b^*\varepsilon}\left[x - \frac{\sinh(x\sqrt{\varepsilon} - L\sqrt{\varepsilon}/4) + \sinh(L\sqrt{\varepsilon}/4)}{\sqrt{\varepsilon}\cosh(L\sqrt{\varepsilon}/4)}\right] \tag{35}$$

In summary, a variational approach was used to re-derive the governing equation and admissible boundary conditions for a beam based on Gurtin-Murdoch surface elasticity theory. The new governing equation is identical to that derived by Liu and Rajapakse (2010) by considering equilibrium of an infinitesimal beam element. The governing equation derived by He and Lilley (2008) has the same structure, but the modified stiffnesses are different from Liu and Rajapakse (2010) and the present study. The admissible boundary condtions are also obtained from the variational formulation, which is identical to the resultant shear and moment at section given by Liu and Rajapakse (2010). On the other hand, the shear force and moment condition used by He and Lilley (2010) were based on the classical beam theory does not agree with the natural boundary condition from the variational formulation. He and Lilley solutions for nanobeams were determined by using essential boundary conditions and these force and/or moment equilibrium conditions at the origin. However, the condition of equilibrium at the beam origin, depending on the beam type, may fail meet the requirement at the other beam end and as a result cantilever beams shows behaviour different from other beams.

ACKNOLEDGEMENT

The work presented in this paper was supported by Grants for New Researcher from Thailand Research Fund (TRF) and Mahidol University (TRG5780139).

REFERENCES

(1) T.Y. Chen, M.S. Chiu and C.N. Weng, "Derivation of the generalized Young–Laplace equation of curved interfaces in nanoscaled solids," J. Appl. Phys., vol. 100, pp.074308, 2006.

(2) J.M. Gere and S.P. Timoshenko, Mechanics of materials, Chapman & Hall, London, England, 1991.

(3) M.E. Gurtin and A.I. Murdoch, "A continuum theory of elastic material surfaces," Arch. Rat. Mech. Anal., vol. 57, pp. 291–323, 1975.

(4) M.E. Gurtin and A.I. Murdoch, "Addenda to our paper: A continuum theory of elastic material surfaces," Arch. Ration. Mech. Anal., vol. 59, pp. 389–390, 1975.

(5) J. He and C.M. Lilley, "Surface effects on the elastic behaviour of static bending nanowires," Nano Letters, vol. 8, pp. 1798-1802, 2008.

(6) P.S. Laplace, Traité de mécanique céleste, Gauthier-Villars, Paris, Vol. 4, Supplements au Livre X, 771-777, 1805.

(7) B. Lee and R.E. Rudd, "First-principles study of the Young's modulus of Si <001> nanowires," Phys. Rev. B, vol. 75, p. 041305(R), 2007.

(8) C. Liu and R.K.N.D. Rajapakse, "Continuum models incorporating surface energy for static and dynamic response of nanoscale beams," Trans. IEEE Nanotechnology, vol. 9, pp. 422–431, 2010.

(9) P. Lu, L.H. He, H.P. Lee and C. Lu, "Thin Plate Theory Including Surface Effects," Int. J. Solids Struct., 43, pp. 4631–4647, 2006.

(10) R.E. Miller and V.B. Shenoy, "Size dependent elastic properties of structural elements," Nanotechnology, vol. 11, pp. 139–147, 2000.

(11) Y. Sapsathiarn and R.K.N.D. Rajapakse, "A model for large deflections of nanobeams and experimental comparison," IEEE Transactions on Nanotechnology, vol. 11, p. 247–254 , 2013.

(12) K. Washizu, Variational methods in elasticity and plasticity, 2nd Ed., New York, Pergamon, 1982.

(13) T. Young, "An Essay on the Cohesion of Fluids," Philos. Trans. R. Soc. London, vol. 95, 65-87, 1805.

Static and dynamic analysis of nanoscale rectangular plates incorporating surface energy

Y. Sapsathiarn[1] and R.K.N.D. Rajapakse[2]

[1] Department of Civil and Environmental Engineering, Faculty of Engineering, Mahidol University, Thailand
[2] Faculty of Applied Sciences, Simon Fraser University, Burnaby, BC V5A 1S6, Canada

In this paper, the Gurtin–Murdoch continuum theory is applied to develop a new continuum mechanics model for static and dynamic analysis of nanoscale rectangular plates. The relevant governing equations are established from basic principles. The analytical static and free vibration solutions of nanoscale rectangular plates are presented. A finite element method for analysis of rectangular nanoplates is also developed in the present paper. Explicit solutions for stiffness and mass matrices and the load vector are derived by using a weighted residual formulation. A selected set of numerical results are presented to investigate the size-dependent static response of nanoscale rectangular plates and the influence of surface properties and boundary conditions.

Keywords: *nanotechnology, nanoplate, surface residual stress, deflection, free vibration*

1 Introduction

Nanoplate structures are key elements used in various nanotechnology-based devices such as nanoelectromechanical systems (NEMS) [1]. To successfully design and manufacture nano-scale devices, a fundamental understanding of their mechanical properties and behavior is required.

Various modeling approaches have been proposed to investigate the behavior of nanostructures. Atomistic simulation [2] have been used by several researchers but the simulation is computationally prohibitive when applied at a device/system level. Continuum mechanics models incorporated with surface energy based on Gurtin and Murdoch has been widely used in the literature for analysis of nanostructures due to their computational efficiency and versatility [3-6]. A nanoplate model based on the Gurtin–Murdoch continuum theory is considered to have bulk material region and an elastic surface with mathematically zero thickness. The surface elastic constants are different from those of bulk and can be determined by atomistic computations and experiments [2].

In this paper, a mechanistic model incorporating the effects of surface energy based on the Gurtin-Murdoch surface elasticity theory [3] is developed to analyze the responses of rectangular nanoplates. A set of closed-form analytical solutions and finite element formulation for static and dynamic analysis of thin rectangular nanoplates are developed in the present paper. Selected numerical results are presented to portray the size-dependent response of rectangular nanoplates and the influence of surface properties and boundary conditions.

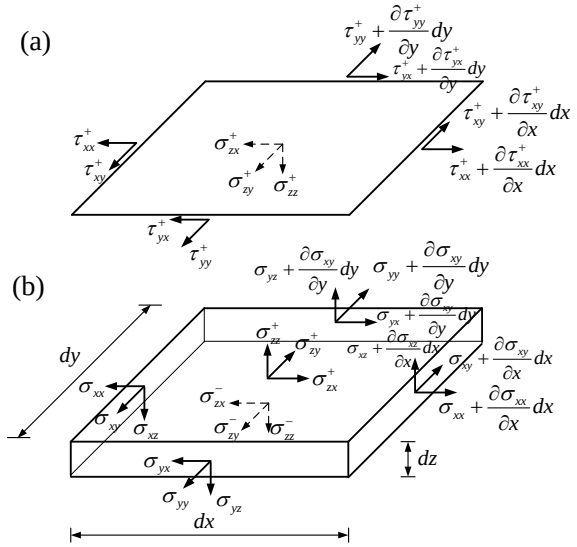

Figure 1: (a) surface stresses on an incremental element of top elastic surface layer and (b) Stress components of an incremental bulk plate element

2 Formulation of rectangular nanoplates governing equations

Consider a thin rectangular plate with Cartesian coordinate system (*x*,*y*,*z*). It is assumed that the response of the plate is governed by the continuum theory proposed by Gurtin and Murdoch [3] and its deflections are small and strains are infinitesimal. An incremental element of the bulk is shown in Fig. 1(b) and the corresponding incremental element of the top surface is shown in Fig. 1(a). The elastic properties of surface

materials are Lamé constants λ_0, μ_0 and surface residual stress under unstrained conditions τ_0, and the mass density of the surface is ρ_0. From Gurtin-Murdoch theory [3],

$$\tau_{\alpha\beta}^{\pm} = \tau_0\delta_{\alpha\beta} + (\mu_0 - \tau_0)\left(u_{\alpha,\beta}^{\pm} + u_{\beta,\alpha}^{\pm}\right) + (\tau_0 + \lambda_0)u_{\gamma,\gamma}^{\pm}\delta_{\alpha\beta} + \tau_0 u_{\alpha,\beta}^{\pm} \quad (1a)$$

$$\tau_{\alpha 3}^{\pm} = \tau_0 u_{3,\alpha}^{\pm} \quad (1b)$$

where $\tau_{\alpha\beta}^{\pm}$ ($\alpha,\beta = x,y$) denotes the surface stress components of the top and bottom surfaces respectively.

The force equilibrium equations of the top surface (Fig. 1(a)) in the *x*- and *y*-directions can be expressed as

$$\frac{\partial \tau_{xx}^{+}}{\partial x} + \frac{\partial \tau_{yx}^{+}}{\partial y} - \sigma_{zx}^{+} = \rho_0 \ddot{u}_x^{+} \quad (2a)$$

$$\frac{\partial \tau_{xy}^{+}}{\partial x} + \frac{\partial \tau_{yy}^{+}}{\partial y} - \sigma_{zy}^{+} = \rho_0 \ddot{u}_y^{+} \quad (2b)$$

where $\sigma_{zi}^{\pm}$ ($i = x,y,z$) is the resulting contact tractions existing on the interface of bulk and top surface layer due to the interaction between the surface layer and bulk. Superscripts + and − are used to denote the field quantities on the top and bottom plate surfaces respectively.

The equation of force equilibrium for an incremental element of the bulk (Fig. 1(b)) in the *x*-direction can be expressed as

$$\int_{-h/2}^{h/2} \frac{\partial \sigma_{xx}}{\partial x} dz + \int_{-h/2}^{h/2} \frac{\partial \sigma_{yx}}{\partial y} dz + \sigma_{zx}^{+} - \sigma_{zx}^{-} + \int_{-h/2}^{h/2} b_x dz = \int_{-h/2}^{h/2} \rho \ddot{u}_x dz \quad (3)$$

where σ_{ij}, b_i and ρ are bulk stresses, body forces and mass density of the bulk material; *h* is the thickness of the plate.

From Fig. 1(b), the force equilibrium equations in the *y*- and *z*-directions and the bending moment equilibrium equations) about the *x*- and *y*-axis can also be obtained. Assumed homogeneous and isotropic, the constitutive relations of the bulk material can be expressed as,

$$\sigma_{xx} = \frac{E}{1-\nu^2}\varepsilon_{xx} + \frac{E\nu}{1-\nu^2}\varepsilon_{yy} + \frac{\nu}{1-\nu}\sigma_{zz} \quad (4a)$$

$$\sigma_{yy} = \frac{E}{1-\nu^2}\varepsilon_{yy} + \frac{E\nu}{1-\nu^2}\varepsilon_{xx} + \frac{\nu}{1-\nu}\sigma_{zz} \quad (4b)$$

$$\sigma_{i\alpha} = 2G\varepsilon_{i\alpha} = \frac{E}{1-\nu^2}\varepsilon_{i\alpha} \quad (4c)$$

In the present paper, σ_{zz} is assumed to vary linearly through the beam thickness and satisfy the equilibrium conditions on the surface,

$$\sigma_{zz} = \frac{1}{2}(\sigma_{zz}^{+} + \sigma_{zz}^{-}) + \frac{z}{h}(\sigma_{zz}^{+} - \sigma_{zz}^{-}) \quad (5)$$

The following displacement functions fields are assumed for Kirchhoff plate,

$$u_x = -z\frac{\partial w}{\partial x};\ u_y = -z\frac{\partial w}{\partial y};\ u_z = w(x,y) \quad (6)$$

The relevant strain-displacement relations are,

$$\varepsilon_{xx} = -z\frac{\partial^2 w}{\partial x^2};\ \varepsilon_{yy} - z\frac{\partial^2 w}{\partial y^2};\ \varepsilon_{xy} - z\frac{\partial^2 w}{\partial x \partial y} \quad (7)$$

and $\varepsilon_{xz} = \varepsilon_{yz} = \varepsilon_{zz} = 0$.

Based on Eqs. (1)-(7), the governing equation for a thin plate including surface effects can be obtained as,

$$D^*\left(\frac{\partial^4 w}{\partial x^4} + 2\frac{\partial^4 w}{\partial x^2 \partial y^2} + \frac{\partial^4 w}{\partial y^4}\right) - 2\tau_0\left(\frac{\partial^2 w}{\partial x^2} + \frac{\partial^2 w}{\partial y^2}\right) + q(x,y) = -(\rho h + 2\rho_0)\frac{\partial^2 w}{\partial t^2} - \left(\frac{\rho^3 h}{12} + \frac{\rho_0 h^2}{2} + \frac{h^2\nu}{6(1-\nu)}\right)\left(\frac{\partial^4 w}{\partial x^2 \partial t^2} + \frac{\partial^4 w}{\partial y^2 \partial t^2}\right) \quad (8)$$

where $D^* = \frac{Eh^3}{12(1-\nu^2)} + \frac{h^2}{2}(2\mu_0 + \lambda_0) - \frac{h^2\tau_0\nu}{6(1-\nu)}$.

3 Analytical solutions

3.1 Static loading of rectangular nanoplate

For the static problems, the governing equation, Eq. (8), is simplified to,

$$D^*\nabla^2\nabla^2 w - 2\tau_0\nabla^2 w + q(x,y) = 0,\quad 0 < x < a,\ 0 < y < b \quad (9)$$

where $\nabla^2 = \frac{\partial^2}{\partial x^2} + \frac{\partial^2}{\partial y^2}$.

Consider a rectangular plate of sides *a* and *b* with all edges simply-supported and subject to a distributed loading of the form

$$q(x,y) = \sum_{m=1}^{\infty}\sum_{n=1}^{\infty} q_{mn} \sin\frac{m\pi x}{a}\sin\frac{m\pi y}{b} \quad (10)$$

Boundary conditions:

$$[w = 0]_{x=0,x=a};\quad [w = 0]_{y=0,y=b} \quad (11a)$$

$$[M_x^* = 0]_{x=0,x=a};\quad [M_y^* = 0]_{y=0,y=b} \quad (11b)$$

where

$$M_x^* = -D^*\frac{\partial^2 w}{\partial x^2} - D_1\frac{\partial^2 w}{\partial y^2} - \frac{h^2\tau_0\nu}{6(1-\nu)}\ddot{w} \quad (12a)$$

$$M_y^* = -D^*\frac{\partial^2 w}{\partial y^2} - D_1\frac{\partial^2 w}{\partial x^2} - \frac{h^2\tau_0\nu}{6(1-\nu)}\ddot{w} \quad (12b)$$

and $D_1 = \dfrac{Eh^3\nu}{12(1-\nu^2)} + \dfrac{h^2}{2}(\lambda_0 + \tau_0)$.

Observing that, since $w = 0$ at all edges (from boundary conditions Eq. (11a)), therefore $\partial^2 w/\partial x^2 = 0$ for the edges parallel to the *x*-axis and $\partial^2 w/\partial y^2 = 0$ for the edges parallel to the y-axis. The deflection function of simply-supported plate can be represented by the double Fourier series

$$w(x,y) = \sum_{m=1}^{\infty}\sum_{n=1}^{\infty} w_{mn} \sin\frac{m\pi x}{a}\sin\frac{n\pi y}{b}, \tag{13}$$

Substituting Eqs. (10) and (13) into Eq. (9) and equating coefficients, the solutions of simply-supported plate can be obtained as

$$w_{mn} = \frac{-q_{mn}}{D^*\pi^4\left(\dfrac{m^2}{a^2}+\dfrac{n^2}{b^2}\right)^2 + 2\tau_0\pi^2\left(\dfrac{m^2}{a^2}+\dfrac{n^2}{b^2}\right)} \tag{14}$$

For a uniform distributed load $q(x,y) = q_0$:

$$q_{mn} = \frac{4q_0}{\pi^2 mn}(1-\cos m\pi)(1-\cos n\pi) \tag{15a}$$

For a concentrated load P_0 at (a', b'):

$$q_{mn} = \frac{4P_0}{ab}\sin\frac{m\pi a'}{a}\sin\frac{m\pi b'}{b} \tag{15b}$$

3.2 Free vibration analysis of rectangular nanoplate

The free vibration characteristics (natural frequencies and mode shapes) of nanoscale plates are an important consideration in the design of NEMS devices. The dynamic response of a simply supported nanoplate can be assumed as

$$w(x,y,t) = \sum_{m=1}^{\infty}\sum_{n=1}^{\infty} w_{mn}\sin\frac{m\pi x}{a}\sin\frac{n\pi y}{b}e^{i\omega t}, \quad 0<x<a,\ 0<y<b \tag{16}$$

Substituting *w* from Eqs. (16) into Eq. (8) yields the characteristic equation of the plate whose roots are the natural frequencies

$$\omega^2 = \frac{D^*\left(\lambda_m^2+\lambda_n^2\right)^2 + 2\tau_0\left(\lambda_m^2+\lambda_n^2\right)}{(\rho h + 2\rho_0) - \left(\dfrac{\rho^3 h}{12} + \dfrac{\rho_0 h^2}{2} + \dfrac{h^2\nu}{6(1-\nu)}\right)\left(\lambda_m^2+\lambda_n^2\right)}, \quad m,n = 1,2,3,... \tag{17}$$

where $\lambda_m = m\pi/a$ and $\lambda_n = n\pi/b$.

4 Finite element formulation

Galerkin's weighted residual method is now applied to Eq. (8) to develop the finite-element (FE) formulation of rectangular nanoscale plates. The weighted residual statement for static loading is [7]

$$0 = \int_V \bar{w}\left\{D^*\left(\frac{\partial^4 w}{\partial x^4} + 2\frac{\partial^4 w}{\partial x^2\partial y^2} + \frac{\partial^4 w}{\partial y^4}\right) - 2\tau_0\left(\frac{\partial^2 w}{\partial x^2} + \frac{\partial^2 w}{\partial y^2}\right) + q(x,y)\right\} dV \tag{18}$$

A 4-node rectangular finite element with *w*, θ_x $[= \partial w/\partial x]$ and θ_y $[= \partial w/\partial y]$ as the nodal variables. The element nodal displacement vector can be written as,

$$\{w^e\} = \begin{bmatrix} w^1 & \theta_x^1 & \theta_y^1 & \dots & w^4 & \theta_x^4 & \theta_y^4 \end{bmatrix}^{\mathrm{T}} \tag{19}$$

The displacement is interpolated by using a set of shape functions as,

$$w = \mathbf{N}\mathbf{w}^e = N_{11}w^1 + N_{12}\theta_x^1 + N_{13}\theta_x^1 + \dots + N_{41}w^4 + N_{42}\theta_x^4 + N_{43}\theta_x^4 \tag{20}$$

where

$$N_{i1} = \frac{1}{8}(1+\xi_0)(1+\eta_0)(2+\xi_0+\eta_0-\xi^2-\eta^2) \tag{21a}$$

$$N_{i2} = \frac{1}{8}\xi_i(\xi_0-1)(1+\eta_0)(1+\xi_0)^2 \tag{21b}$$

$$N_{i3} = \frac{1}{8}\eta_i(\eta_0-1)(1+\eta_0)(1+\eta_0)^2 \tag{21c}$$

$$\xi = \frac{x-x_0}{a};\ \eta = \frac{y-y_0}{b};\ \xi_0 = \xi\xi_i;\ \eta_0 = \eta\eta_i \tag{21d}$$

in which (x_0, y_0) are the global coordinates of the center of the rectangle and

Substitution of Eq. (20) into Eq. (18), the finite element model of nanoscale rectangular plate is obtained by

$$[K^e]\{w^e\} = \{F^e\} \tag{22}$$

where

$$\mathbf{K}^e = \int_{\Omega_0}\left\{\mathbf{B}_2{}^T\mathbf{C}\mathbf{B}_2 + 2\tau_0\mathbf{B}_1{}^T\mathbf{B}_1\right\}dxdy; \tag{23a}$$

$$\mathbf{F}^e = \int_{\Omega_0}\mathbf{N}q\,dxdy;\ \mathbf{C} = D^*\begin{bmatrix} 1 & \nu & 0 \\ \nu & 1 & 0 \\ 0 & 0 & (1-\nu)/2 \end{bmatrix} \tag{23b}$$

$$\mathbf{B}_1 = \begin{bmatrix} \dfrac{\partial N_{11}}{\partial x} & \dfrac{\partial N_{12}}{\partial x} & \dfrac{\partial N_{13}}{\partial x} & \dots & \dfrac{\partial N_{41}}{\partial x} & \dfrac{\partial N_{42}}{\partial x} & \dfrac{\partial N_{43}}{\partial x} \\ \dfrac{\partial N_{11}}{\partial y} & \dfrac{\partial N_{12}}{\partial y} & \dfrac{\partial N_{13}}{\partial y} & \dots & \dfrac{\partial N_{41}}{\partial y} & \dfrac{\partial N_{42}}{\partial y} & \dfrac{\partial N_{43}}{\partial y} \end{bmatrix} \tag{23c}$$

$$\mathbf{B}_2 = \begin{bmatrix} \dfrac{\partial^2 N_{11}}{\partial x^2} & \dfrac{\partial^2 N_{12}}{\partial x^2} & \dfrac{\partial^2 N_{13}}{\partial x^2} & \dots & \dfrac{\partial^2 N_{41}}{\partial x^2} & \dfrac{\partial^2 N_{42}}{\partial x^2} & \dfrac{\partial^2 N_{43}}{\partial x^2} \\ \dfrac{\partial^2 N_{11}}{\partial y^2} & \dfrac{\partial^2 N_{12}}{\partial y^2} & \dfrac{\partial^2 N_{13}}{\partial y^2} & \dots & \dfrac{\partial^2 N_{41}}{\partial y^2} & \dfrac{\partial^2 N_{42}}{\partial y^2} & \dfrac{\partial^2 N_{43}}{\partial y^2} \\ 2\dfrac{\partial^2 N_{11}}{\partial x\partial y} & 2\dfrac{\partial^2 N_{12}}{\partial x\partial y} & 2\dfrac{\partial^2 N_{13}}{\partial x\partial y} & \dots & 2\dfrac{\partial^2 N_{41}}{\partial x\partial y} & 2\dfrac{\partial^2 N_{42}}{\partial x\partial y} & 2\dfrac{\partial^2 N_{43}}{\partial x\partial y} \end{bmatrix} \tag{23d}$$

5 Numerical solutions

The analytical solutions and FE formulation presented in the previous sections are implemented in a computer code to analyze rectangular nanoscaled plates. Plate made of aluminium (Al) and silicon (Si) are used in the numerical study. The relevant bulk material properties are E = 90 GPa, ν = 0.23 for Al and E = 107 GPa, ν = 0.33 for Si [2]. The surface material properties for a [100] surface of these materials are τ_0 = 0.5689 N/m, μ_0 = -5.4251 N/m, λ_0 = 3.4939 N/m, $\rho = 2.7\times10^3$ kg/m^3 and $\rho_0 = 5.46\times10^{-7}$ kg/m^2 for Al and $\tau_0 = 0.6056$ N/m, μ_0 = -2.7779 N/m, λ_0 = -4.4939 N/m, $\rho = 2.33\times10^3$ kg/m^3 and $\rho_0 = 3.17\times10^{-7}$ kg/m^2 for Si [2].

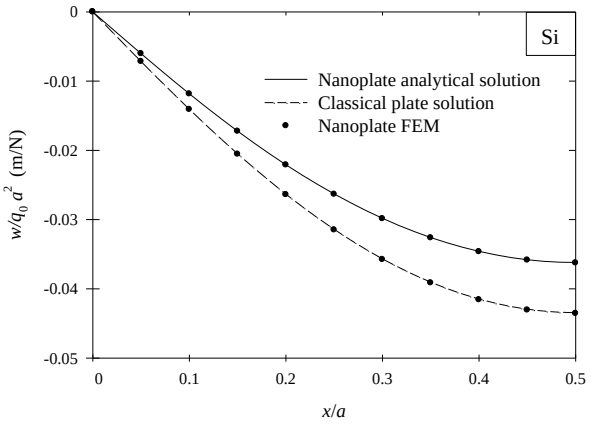

Figure 2: Deflection profiles of plates with all edges simply-supported under uniformly distributed load (a = 200 nm, b = 200 nm, h = 10 nm)

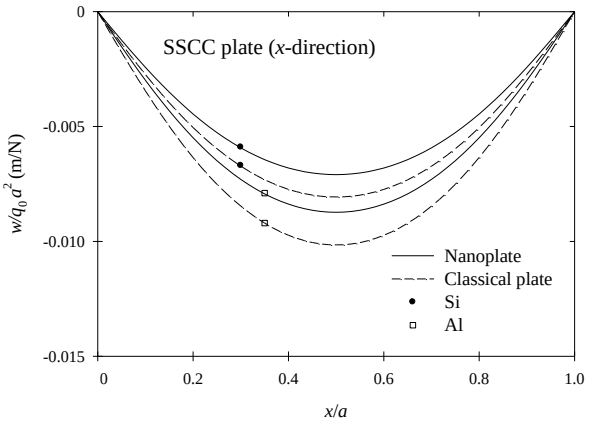

Figure 3: Deflection profiles of SSCC plate under uniformly distributed load (a = 200 nm, b = 200 nm, h = 10 nm)

Deflection profile of Si nanoplate with all edges simply-supported under uniformly distributed load q_0 is presented in Fig. 2. Classical plate solutions [8] for identical plates (zero surface material parameters) are also shown in these figures to assess the influence of surface energy. Static deflections of Si nanoplate is lower than the classical plate model. This implies that surface energy effects incorporated in the nanoplate model make the plates stiffer. Figure 3 shows the deflection profiles of Al and Si plates with two opposite edges simply supported and the other two edges clamped (SSCC). Compared to the simply-supported plate (Fig. 2), surface energy effect causes a similar stiffening behavior, although less prominent. The main contribution for the deviated responses between the classical and nanoscale plates is due to the surface material parameters μ_0, λ_0 and τ_0.

6 Conclusion

A mechanistic model incorporating the effects of surface energy based on the Gurtin-Murdoch surface elasticity theory is proposed to analyze the responses of rectangular nanoplates. A set of closed-form analytical static and free vibration solutions of nanoscale rectangular plates are presented. A finite element formulation for thin rectangular nanoplates are successfully developed. Selected numerical results are presented to portray the size-dependent response of rectangular nanoplates and the influence of surface properties and boundary conditions.

Acknowledgments

The work presented in this paper was supported by the Natural Sciences and Engineering Research Council of Canada (NSERC) and the Grant for New Researcher from Thailand Research Fund and Mahidol University (TRG5780139).

References

[1] Craighead, H.G., Nanoelectromechanical Systems, *Science*, Vol. 290, p. 1532-1535, 2000.

[2] Miller, R.E. and Shenoy, V.B., Size-Dependent Elastic Properties of Nanosized Structural Elements, *Nanotechnology*, Vol. 11, p. 139-147, 2000.

[3] Gurtin, M.E. and Murdoch, A.I., A Continuum Theory of Elastic Material Surfaces, *Archive for Rational Mechanics and Analysis*, Vol. 57, p. 291-323, 1975.

[4] He, L.H., Lim, C.W. and Wu, B.S., A Continuum Model for Size-Dependent Deformation of Elastic Films of Nano-Scale Thickness, *International Journal of Solids and Structures*, Vol. 41, p. 847-857, 2004.

[5] Sapsathiarn, Y. and Rajapakse, R.K.N.D., A Model for Large Deflections of Nanobeams and Experimental Comparison, *IEEE Transaction on Nanotechnology*, Vol. 11, p. 247–254, 2012.

[6] Liu, C. and Rajapakse, R.K.N.D., A Size-dependent Continuum Model for Nanoscale Circular Plates, *IEEE Transaction on Nanotechnology*, Vol. 12, p. 13-20, 2013.

[7] Zienkiewicz, O.C., and Taylor, R.L., *The Finite Element Method*, Butterworth-Heinemann, Boston, 2000.

[8] Timoshenko, S.P. and Woinowsky-Krieger, S., *Theory of Plates and Shells*, McGraw Hill, New York, 1959.